Supporting Information for

Lanthanide complexes bearing a bioinspired Cu^{II}-binding site with picomolar affinity: synthesis, structural, relaxometric and luminescence studies

Katharina Zimmeter[a], Bertrand Vileno[a], Agnès Pallier[b], Carlos Platas-Iglesias[c], Peter Faller[a,d], Célia S. Bonnet[b]*, Angélique Sour[a]*

[a]Institut de Chimie (UMR 7177), Université de Strasbourg – CNRS, 4 Rue Blaise Pascal, 67000 Strasbourg, France.

[b] Centre de Biophysique Moléculaire, Université d´Orléans, Orléans, France

[c] Departamento de Química Fundamental, Universidade da Coruña, Campus da Zapateira, Rúa da Fraga 10, 15008 A Coruña, Spain.

[d] Institut Universitaire de France (IUF), 1 rue Descartes, 75231 Paris, France.

celia.bonnet@cnrs-orleans.fr ; a.sour@unistra.fr

1. Synthesis

Reagents: All reagents were purchased from commercial sources and used without further purification. Diisopropyl ethylamine (DIEA), triethyl amine (TEA), piperidine, acetic anhydride, trifluoroacetic acid (TFA), triisopropyl silane (TIS), Fmoc-His(Trt)-OH, tri-tert-butyl 2,2',2''-(1,4,7,10-tetraazacyclododecane-1,4,7-triyl)triacetate (DO3A*t*Bu), 1-[bis(dimethylamino)methylene]-1H-1,2,3-triazolo[4,5-b]pyridinium 3-oxide hexafluorophosphate (HATU), *N*,*N*'-diisopropylcarbodiimide (DIC), Oxyma Pure, 1,8-diazabicyclo[5.4.0]undec-7-ene (DBU), pyridine-2,6-dicarboxylic acid, ethyltrifluoroacetate, pyropylamine hydrochloride, 3-bromopropylamine hydrobromide, 2,4,6-trinitrobenzene-1-sulfonic acid (TNBS). Rink Amide MBHA resin (100-200 mesh, 0.7 mmol/g) was purchased from Iris Biotech.

Solid phase peptide synthesis (SPPS) was performed on a Rink Amide AM resin (100-200 mesh, loading 0.70 mmol/g) on a 0.1 mmol reaction scale. All steps were carried out in a syringe with a filter frit under continuous shaking on a CAT shaking device at room temperature. The resin was swelled in DCM for 20 min, then in DMF for 15 min. Fmoc deprotection was performed 4 times using 5 mL of a solution of 20% piperidine in DMF each time. The coupling of Fmoc-His(Trt) was performed for 1 hour using 2 eq. of the amino acid, 1.9 eq. HBTU, 4 eq. DIEA in 3-10 mL DMF. The conditions of the coupling steps involving pyridine-2,6-dicarboxylate are described in detail below. TNBS test was performed after the coupling steps to evaluate if they have been complete. Capping of unreacted amines was performed using a solution of 5% acetic anhydride and 10% DIEA in DMF (5 min). The Fmoc deprotection was followed by UV-Vis absorption spectroscopy (ε_{301nm} = 7800 $M^{-1}s^{-1}$). Before the cleavage, the resin was washed three times each with DMF, DCM and diethyl ether and dried. Cleavage from the resin and removal of the protecting groups were performed using a solution of TFA / TIS / H_2O (95/2.5/2.5) (3 x 3 mL for 30 min). TFA was removed by evaporation, the crude was solubilized in ACN/ H_2O and lyophilized.

NMR spectra were recorded on Bruker AVANCE 300, 500 spectrometers in deuterated solvents ($CDCl_3$ and MeOD-d_4) The peak of the solvent was used as a reference and the chemical shifts are given in parts per million (ppm) and *J* values in Hertz (Hz). The multiplicity of the signals is abbreviated as followed: singlet (s), doublet (d), triplet (t), doublet of doublets (dd), triplet of quartets (tq), doublet of doublets of doublets (ddd). Broad signals are indicated by broad (br.). The attribution of the signals was performed with the help of 2D spectra (^{1}H-^{1}H COSY, HSQC and HMBC) for the end products and by analogy for the intermediates.

Mass spectrometry (MS): LC-MS analysis was carried out on a Agilent 1100 Series LC-system with a XBridge® Peptide BEH C18 Column (300 Å, 3.5 µm, 4.6 mm x 150 mm, 1/pkg) combined with an Agilent 6120 Quadrupol mass detector or on a Thermo Scientific Accela UHPLC with a Hypers II GOLD C18 column (50 x 2.1 mm^2, 1.9 µm) combined with a Thermo Scientific LCQ Fleet ion-trap. HR-MS analysis was carried out in the mass service of the chemistry faculty on a ORBITRAP HR-MS (Thermofisher) with electrospray ionization or on a MALDI Autoflex II TOF/TOF (Bruker).

HPLC: Purification was performed on preparative HPLC (XBridge Peptide BEH C18 OBD Prep Column from Waters, 19 mm x 150 mm, pore size 130 Å, particle size 5 µm) and a flow rate of 1 mL/min, using H_2O + 0.1% TFA (Eluent A) and 0.1% TFA in 90% ACN, 10% H_2O (Eluent B) as eluents. UV-Vis detection was carried out at 214 and 254 nm.

Salt exchange was performed using a 2 mM aqueous HCl solution followed by lyophilization. This process was repeated 3 to 4 times to ensure thorough exchange. The volume of the HCl solution added was chosen to ensure an excess of HCl relative to the TFA counterions in the sample.

1.1 Synthesis of DO3A-C3AmpicH and the corresponding lanthanide complexes

N-(3-Bromopropyl)-2,2,2-trifluoroacetamide 1

Compound **1** was synthesized following the protocol described by Seibel and coll.[1] It was used for the next step without column chromatography purification.

Compound 2

Compound **1** (351 mg, 1.5 mmol, 1 eq), DO3AtBu (643 mg, 1.25 mmol, 0.83 eq.) and K_2CO_3 (518 mg, 3.75 mmol, 2.5 eq.) were dissolved in anhydrous ACN (6 mL) and stirred at 70°C under argon atmosphere for 24 h. The reaction progress was controlled by LC-MS analysis. After cooling to room temperature, K_2CO_3 was removed by filtration and the solvents were removed by evaporation. The crude was then purified by silica gel chromatography (eluted with a gradient of MeOH (2-20%) in DCM containing 2% aqueous NH_3) to give 405 mg (49%) of compound **2**.

^{1}H-NMR ($CDCl_3$, 300 MHz) δ 1.6-3.5 (m, 28 H, CH_2) 1.42-1.47 m, 27 H, $C(CH_3)_3$) ppm.

LC-ESI-MS: m/z for $[M+H]^+$: calcd. 668.41, found: 668.20.

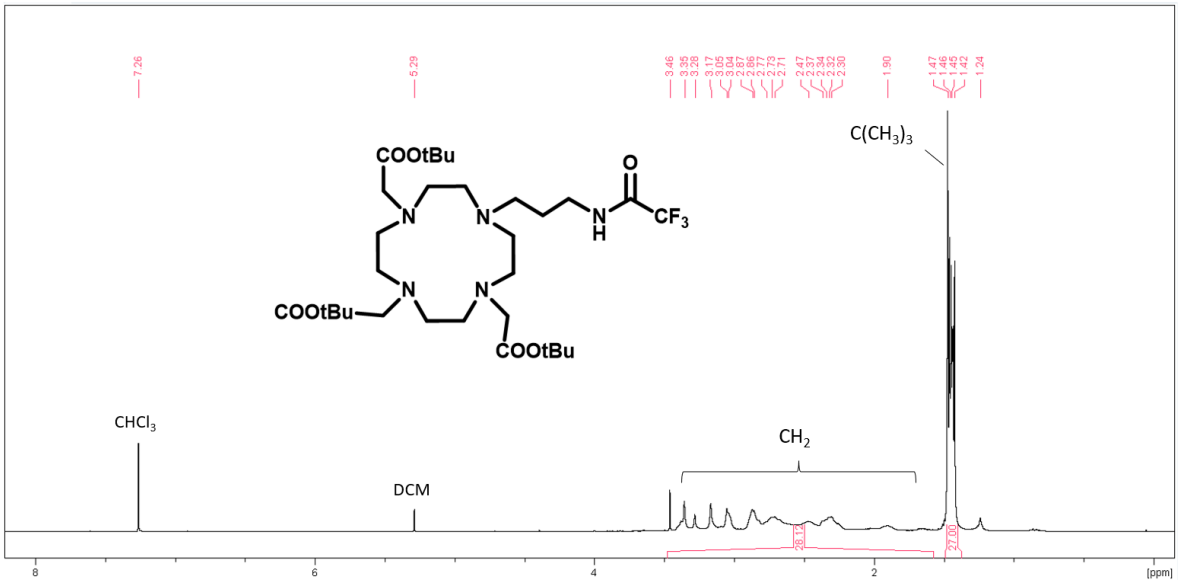

Figure S1: ^{1}H-NMR spectrum of compound **2** (300 MHz, $CDCl_3$).

Compound 3

To a solution of compound **2** (248 mg, 0.37 mmol, 1 eq) in EtOH (7.5 mL) was added an aqueous NaOH solution (2.5 mL, 0.3 M) and the mixture was stirred at room temperature for 5 h. After evaporation of the solvents, the product was solubilized in DCM (10 mL) and washed with an aqueous NaOH solution (pH 12, 3 times, 3 mL). The organic phase was dried over Na_2SO_4 and evaporated. The reaction was considered quantitative (211 mg).

^{1}H-NMR ($CDCl_3$, 300 MHz) δ: 8.24 (s, 2H, NH_2), 2.6-3.3 (m, 26 H, CH_2), 1.60 (m, 2 H, CH_2), 1.42-1.44 (m, 27 H, $C(CH_3)_3$) ppm.

LC-ESI-MS: m/z for $[M+H]^+$ calcd: 572.43, found: 572.22.

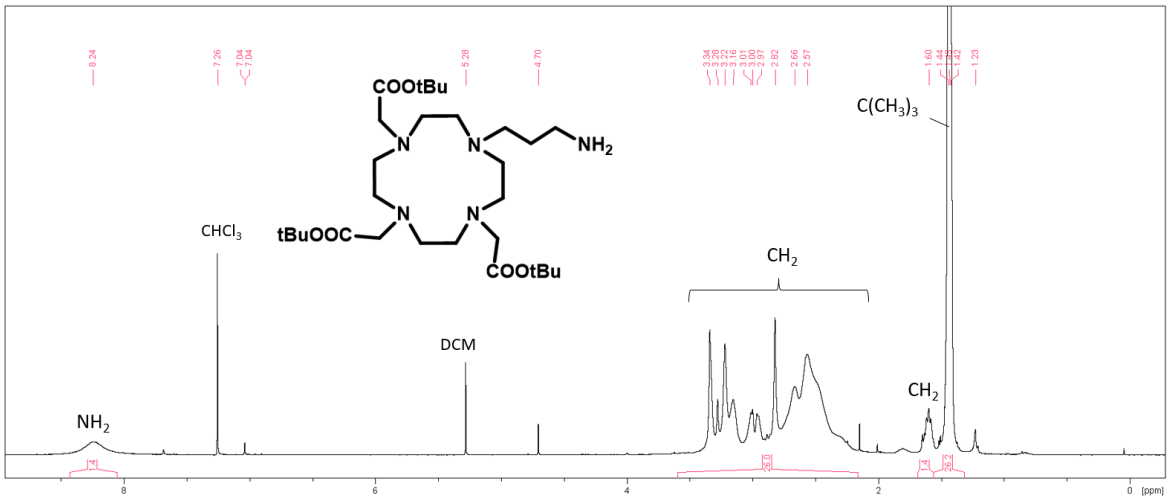

Figure S2: ^{1}H-NMR spectrum of compound **3** (300 MHz, $CDCl_3$).

Compound 4

To a solution of pyridine-2,6-dicarboxylate (187 mg, 1.12 mmol, 4 eq.) in DMF (3 mL), Oxyma Pure (80 mg, 0.56 mmol, 2 eq.) and DIC (87 µL, 0.56 mmol, 2 eq) were added. After 2 min, this solution was added to compound **3** (159 mg, 0.28 mmol, 1 eq.) and the resulting dark yellow suspension was stirred at room temperature for 3 days. After removal of the DMF, the crude was purified by silica gel chromatography (eluted with a gradient of MeOH (2-20%) in DCM containing 2% aqueous NH_3). As the separation of the starting compound **3** from the product **4** turned out to be very difficult, the crude (271 mg) was engaged in the next step without further purification. The NMR spectrum shows thus a mixture (approximately 1:1) of **3** and **4**. The yield of the reaction is estimated to be between 40-50%.

LC-ESI-MS: m/z for $[M+H]^+$ calcd: 721.44, found: 721.33.

Compound DO3A-C3AmpicH

The synthesis of **DO3A-C3AmpicH** was carried out on Rink amide AM resin on a 0.1 mmol scale. Fmoc-His(Trt)-OH was attached to the resin following the standard SPPS protocol. The following coupling step with **4** (216 mg, 0.3 mmol, 3 eq.) was performed using the activator HATU (99 mg, 0.26 mmol, 2.6 eq.) and the base DIEA (105 µL, 0.6 mmol, 6 eq.) in DMF (2.5 mL). The reaction was carried out for 24 h at RT. Since the TNBS test indicated that the reaction was not complete, the reaction was repeated for an additional 24 hours using a fresh solution of compound **4**, activator and base. After cleavage from the resin and evaporation of the TFA, purification was performed on preparative RP-HPLC (5% eluent B: isocratic for 3 min, 5-15% in 8 min, 2 min isocratic at 15% B). The product was obtained in 50 % yield with over 95% purity (34 mg).

^{1}H NMR (CD_3OD, 500 MHz) δ 8.74 (br. s, 1 H, Im-H1), 8.25 (dd, *J*=1.2 Hz, *J*=7.8 Hz, 1H, Pyr-H3 or Pyr-H5), 8.18 (dd, *J* =09 Hz, *J* =7.8 Hz, 1H, Pyr-H3 or Pyr-H5), 8.10 (dd, *J* =7.8 Hz, *J* =7.8 Hz, 1H, Pyr-H4), 7.42 (br. s, 1H, Im-H2), 5.03 (dd, *J* =5.2 Hz, *J* =9.4 Hz, 1H, CH), 4.09 (br. s, 2H, CH_2), 3.74-2.97 (m, 28H, CH_2s), 2.29-2.11 (m, 2H, CH_2) ppm.

^{13}C NMR (CD_3OD, 125 MHz) δ 174.9 and 174.7 (Amide-His), 166.2 and 165.8 (Amide-pic), 150.2 and 149.7 (Pyr-C), 140.5 (Pyr-CH4), 134.8 (Im-H1), 131.8 (Im-C), 126.3 (Pyr-CH3 and Pyr-CH5), 118. 5 (Im-CH2), 55.6 (CH_2), 54.1 (CH_2), 54.1 (CH_2), 53.5 (CH), 53.1 (CH_2), 51.3 (CH_2), 50.2 (CH_2), 50.1 (CH_2), 49.6 (CH_2), 49.5 (CH_2), 49.3 (CH_2), 49.1 (CH_2), 48.9 (CH_2), 37.9 (CH_2), 28.0 (CH_2-1), 25.1 (CH_2) ppm.
The signals of the quaternary carbons of the DOTA carboxylic acids are not visible in the ^{13}C-NMR, longer acquisition times would have been necessary.

HR-ESI-MS: m/z for $[M+K]^+$: calcd: 689.3365, found: 689.3379.

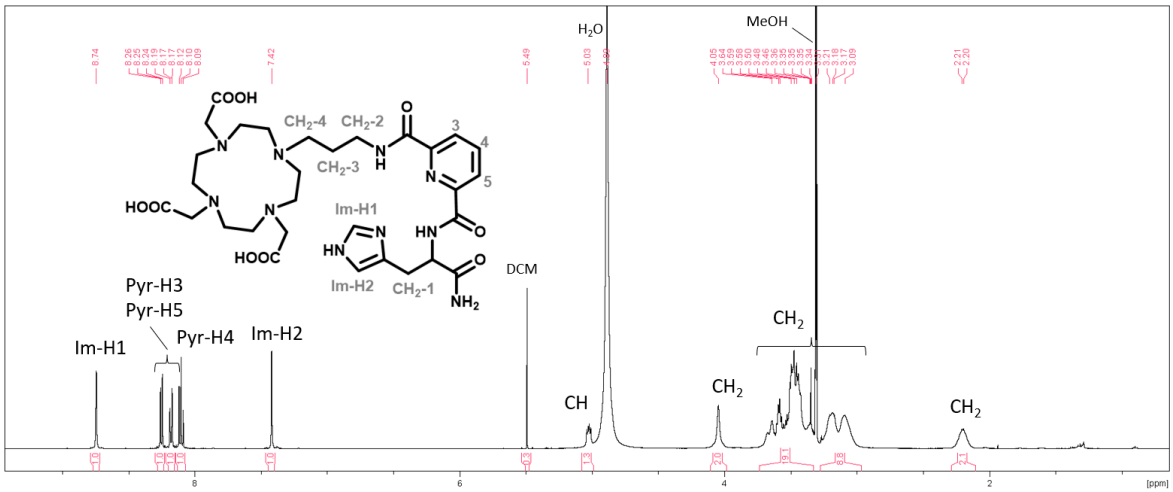

Figure S3: ^{1}H-NMR spectrum of DO3A-C3AmpicH (500 MHz, CD_3OD).

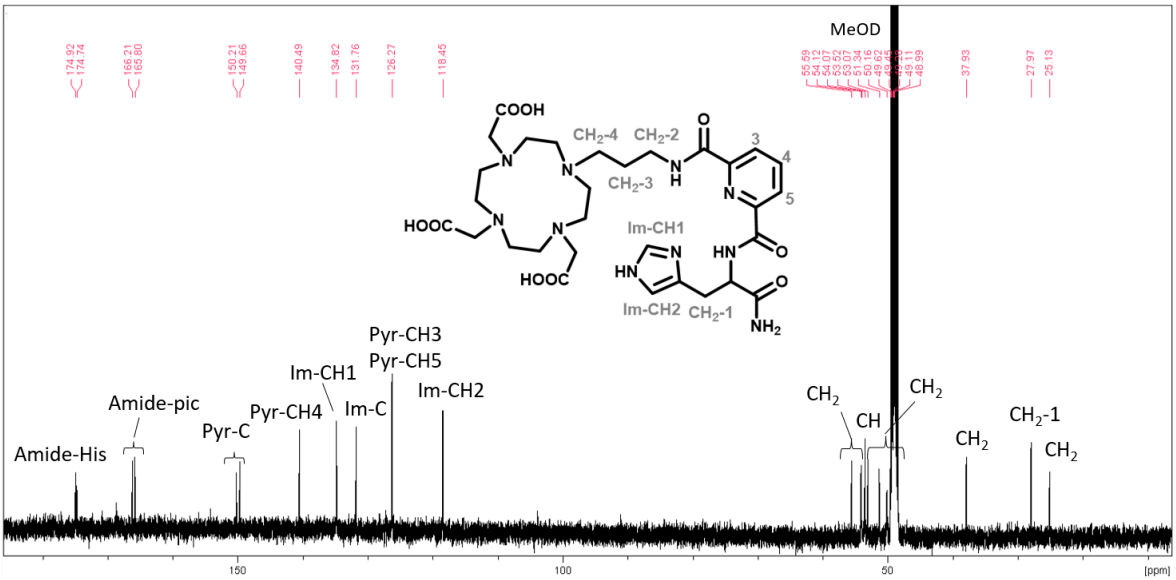

Figure S4: ^{13}C-NMR spectrum of DO3A-C3AmpicH (125 MHz, CD_3OD).

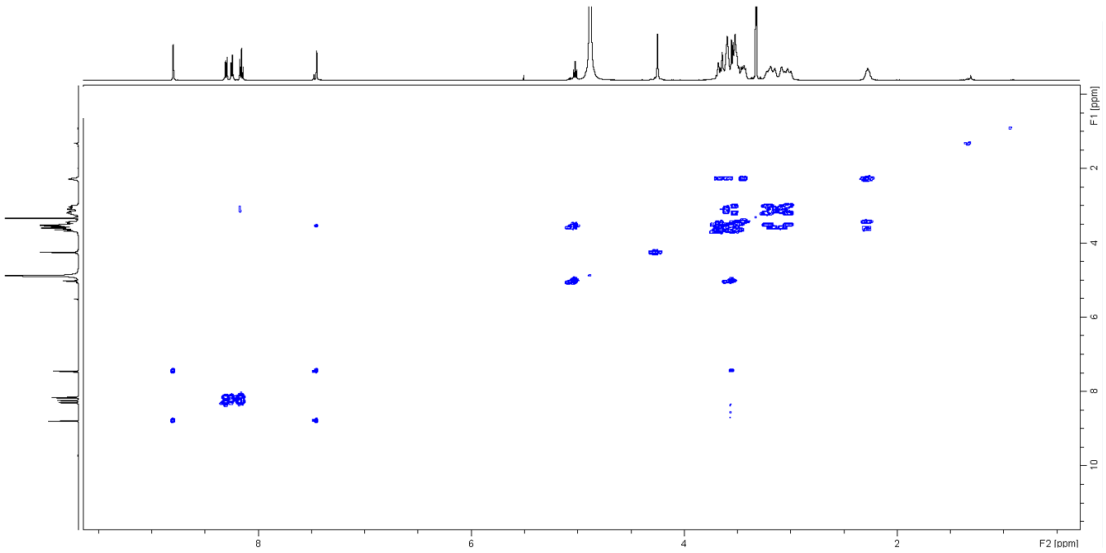

Figure S5: ^{1}H ^{1}H-COSY spectrum of DO3A-C3AmpicH (500 MHz, CD_3OD).

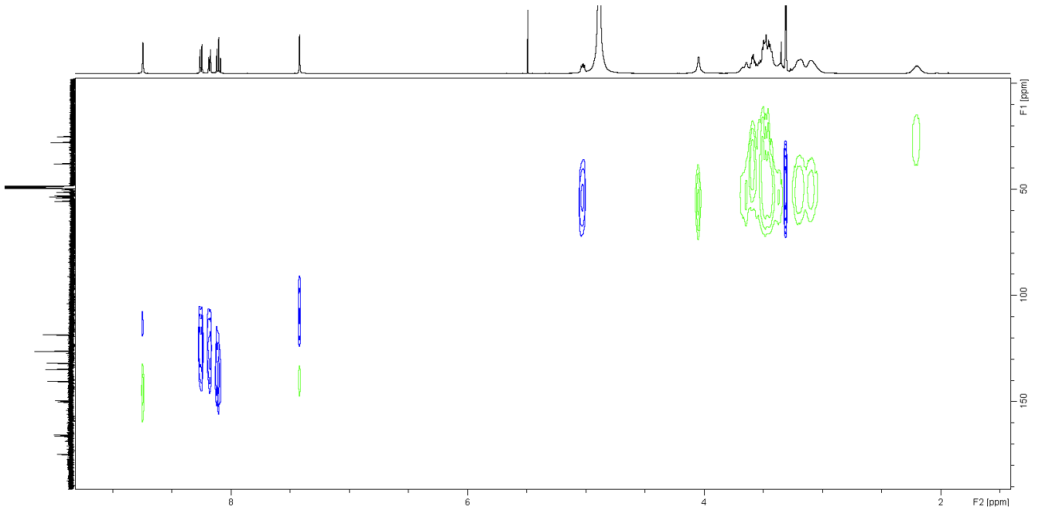

Figure S6: HSQC spectrum of DO3A-C3AmpicH (500 / 125 MHz, CD_3OD).

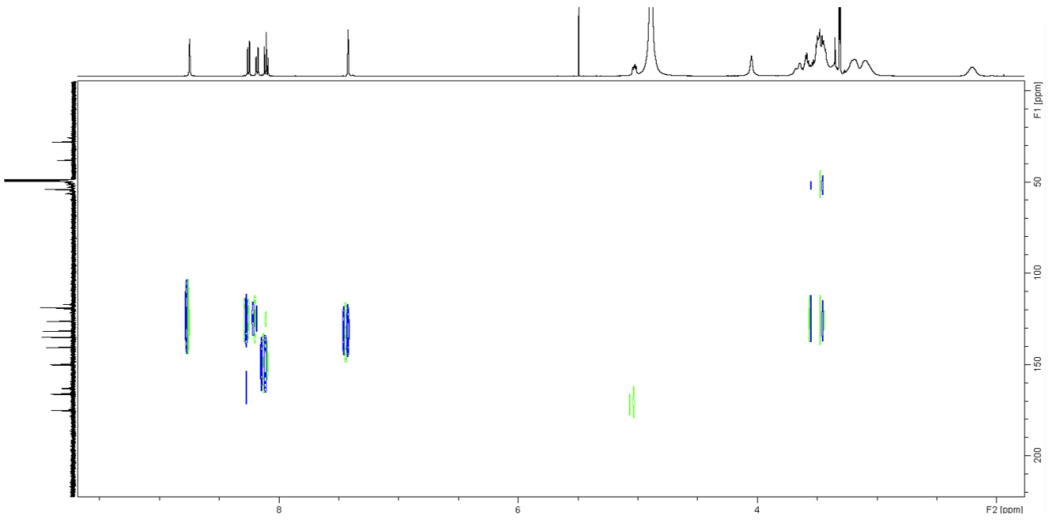

Figure S7: HMBC spectrum of DO3A-C3AmpicH (500 / 125 MHz, CD_3OD).

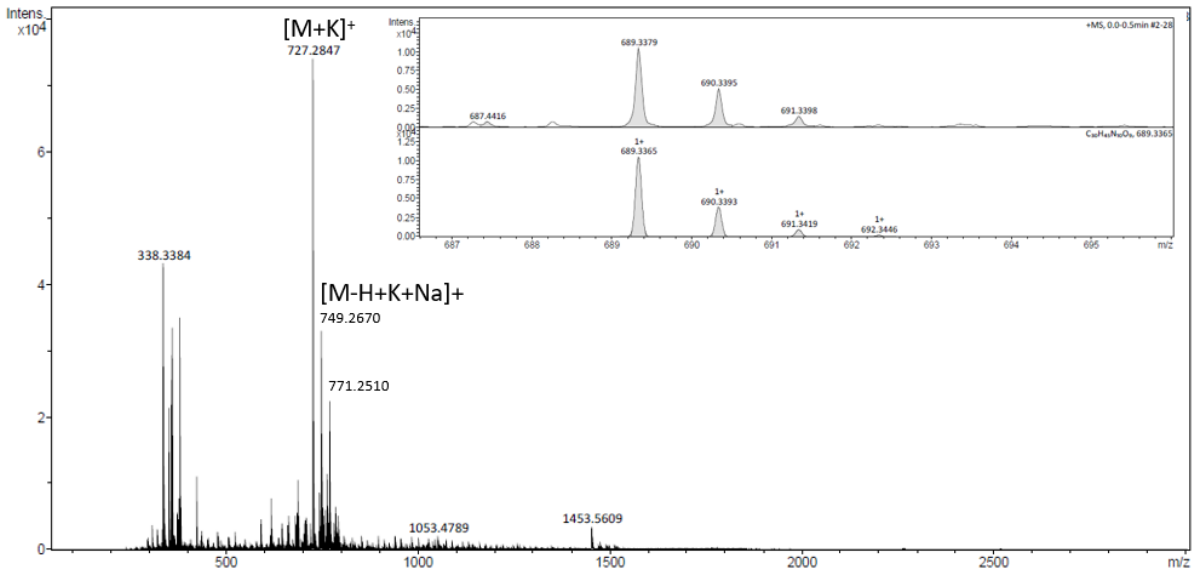

Figure S8a: HR-ESI-MS spectrum of DO3A-C3AmpicH.

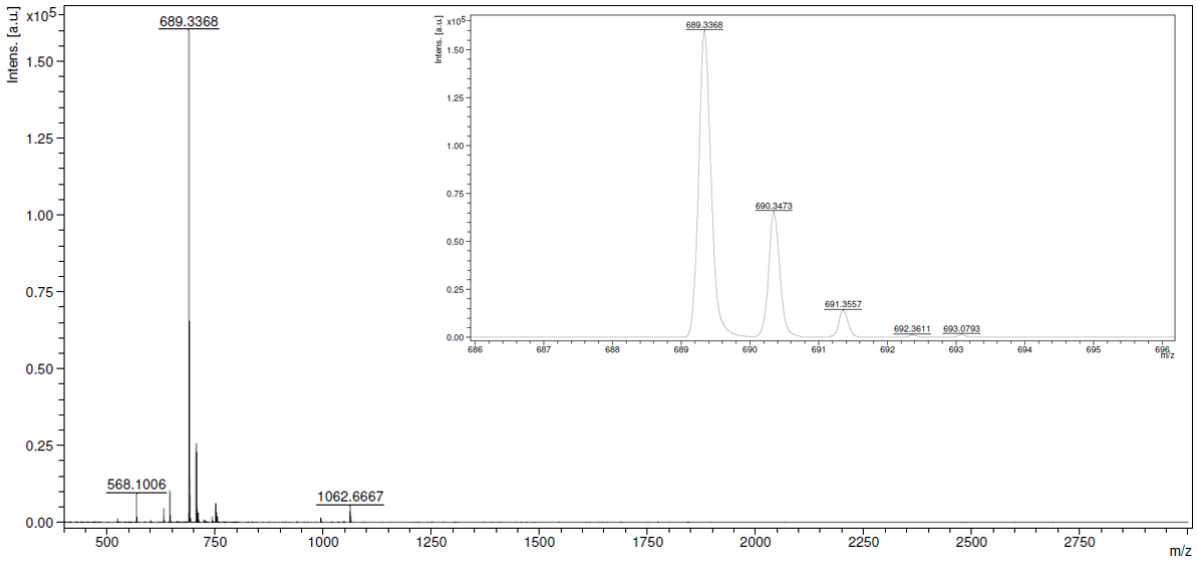

Figure S8b: MALDI TOF MS spectrum of DO3A-C3AmpicH.

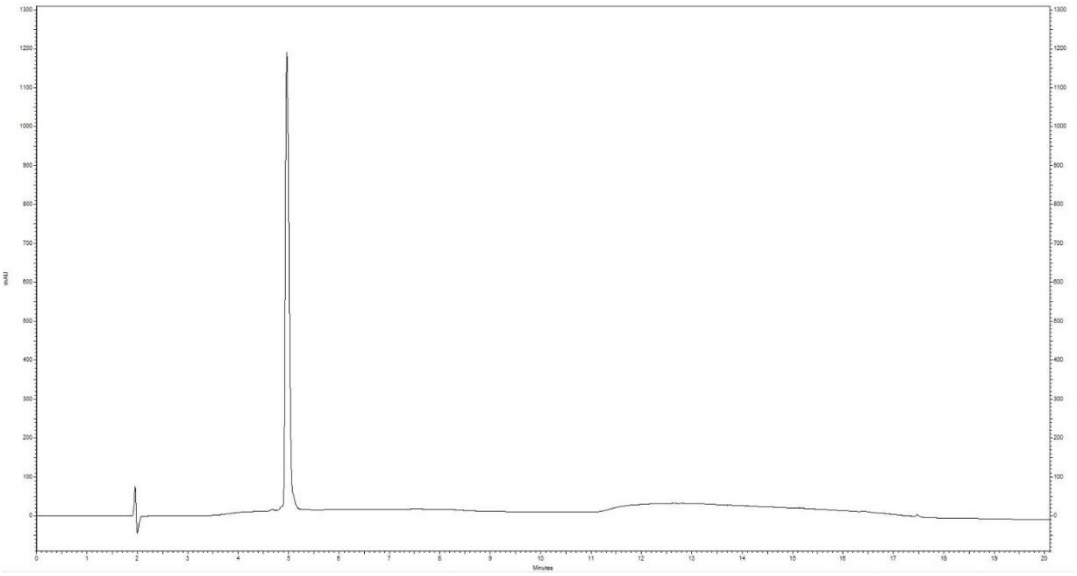

Figure S9: RP-HPLC of DO3A-C3AmpicH. Gradient: 5-22% eluent B in 5 min, plateau at 22% for 3 min, 22-100% in 7 min.

Lanthanide complexes

The formation of the lanthanide complexes was performed by the stepwise addition of $EuCl_3$ or $GdCl_3$ to the ligand, adjusting the pH between 5.0 and 6.5 with NaOH and HCl, and incubation at 40-50°C for a minimum of 3 hours. The presence of free Gd^{III} or Eu^{III} was assessed using Xylenol Orange. 5 µL of the complex solution was mixed with 700 µL of urotropine buffer (100 mM, pH 5.8, pH adjusted with NaOH) and 10 µL of Xylenol Orange solution (3 mg/mL, pH 5.8, pH adjusted with NaOH). The appearance of a purple colour indicated the presence of free lanthanide ions. Positive and negative controls were carried out for comparison. If no free lanthanide ions were detected, an additional aliquot of the lanthanide solution was added. In the opposite case, more ligand solution was added and the incubation and Xylenol Orange assay were repeated until maximum ligand complexation was achieved without excess free lanthanide ions. This method ensures that a maximum of 5% of free ligand is present in the sample. The concentrations of Ln^{III}-containing solutions were also checked by ICP-OES (Inductively Coupled Plasma Optical Emission Spectrometry) or BMS (bulk magnetic susceptibility) measurements when possible.

HR-ESI-MS :

For Gd-DO3A-C3AmpicH:
m/z for $[M+H]^+$: calcd. 844.2372, found: 844.2369.
m/z for $[M+2H]^{2+}$: calcd. 422.6222, found: 422.6254.

For Eu-DO3A-C3AmpicH:
m/z for $[M+H]^+$: calcd. 839.2344, found: 839.2344 (same value).

Sample Name: ZK37Eu Analysis Name: I20250821-04
ThermoFisher Orbitrap: Exactive Plus with Extend Mass Range: Source HESI II Ion Polarity: Positive
Analysis Name: I20250821-04

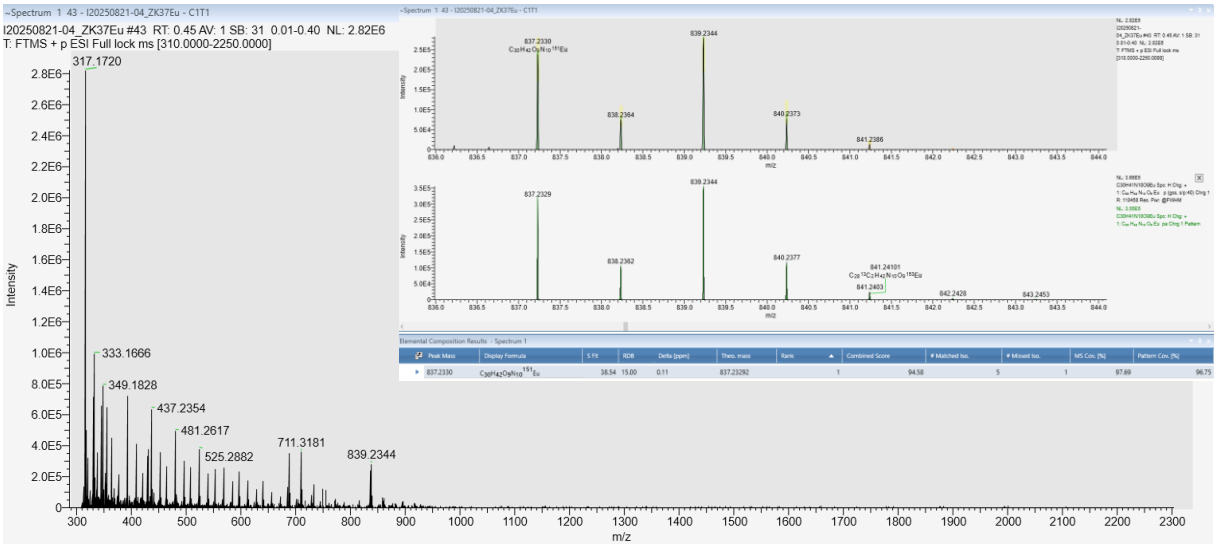

Figure HRMS Eu: HR-ESI-MS spectrum of Eu-DO3A-C3AmpicH.

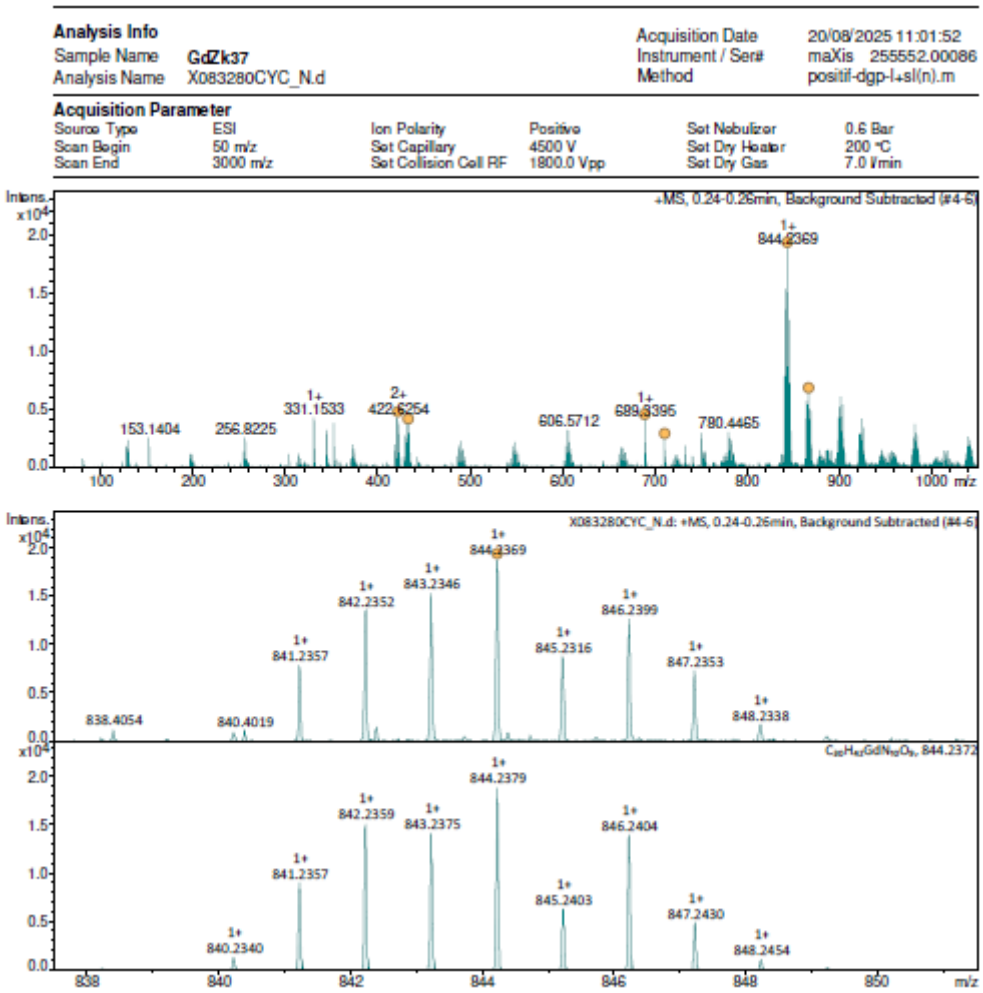

Figure HRMS Gd: HR-ESI-MS spectrum of Gd-DO3A-C3AmpicH.

1.2 Synthesis of C3AmpicH

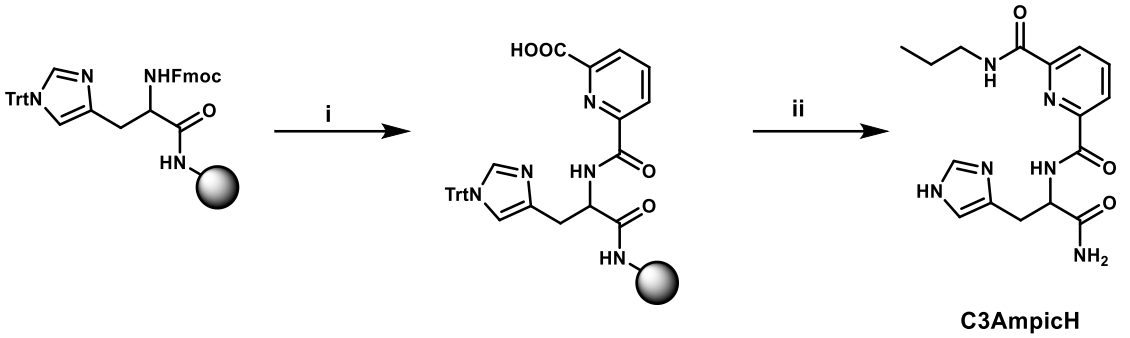

Scheme S1: Synthesis scheme of C3-AmpicH. Conditions: **i)** 1 eq. DIC, 1 eq. Oxyma Pure, 2 eq. pyridine-2,6 dicarboxylic acid, DMF, RT, 3 h. **ii)** 1) 4 eq. propylamine hydrochloride, 1 eq. DIC, 1 eq. Oxyma Pure, DMF, 4 eq. DBU, (3 x 3-4 h), 2) TFA/TIS/H_2O: 95/2.5/2.5, 3 x 30 min. The grey spheres symbolize the Rink Amide AM resin.

The ligand C3AmpicH was synthesized on Rink amide AM resin on a 0.1 mmol scale (143 mg, loading: 0.70 mmol/g). The coupling step between pyridine-2,6-dicarboxylic acid and the histidine on the resin was performed using pyridine-2,6-dicarboxylic acid (33 mg, 0.2 mmol, 2 eq.), DIC (16 µL, 1 eq., 0.1 mmol) and Oxyma Pure (14 mg, 1 eq., 0.1 mmol) in DMF (3 mL) with a reaction time of 3 h. It has been noticed, that washing steps before this step were very important to prevent the presence of piperidine from the Fmoc deprotection solution, which could react with the second carboxylic acid of the reactant. Also, DIEA was avoided, as its use in this reaction step led to undesired side products, possibly due to the reaction of DIEA degradation products with the second carboxylic acid function. A microcleavage followed by LC-MS analysis confirmed the formation of the right intermediate. For the following coupling step with propylamine hydrochloride, the carboxylic acid on the resin was first pre-activated for 20 min with DIC (16 µL, 0.1 mmol, 1 eq.) and Oxyma Pure (14 mg, 0.1 mmol, 1 eq.) in DMF. Then a solution of propyl amine hydrochloride (38 mg, 0.4 mmol, 4 eq.) and DBU (119 µl, 0.8 mmol, 8 eq.) in DMF was added. This step was performed 3 times for each 3-4 h with a fresh solution at each time. After cleavage from the resin, the crude was purified by RP-HPLC using a gradient of 10-60% eluent B in 15 min. 21 mg of pure product were obtained as a white powder after salt exchange (57% yield, considering 1 Cl^- counterion).

HR-ESI-MS m/z for $[M+H]^+$: calcd. 345.1670, found: 345.1674.

NMR ^{1}H (300 MHz, CD_3OD): δ 8.79 (d, *J* = 1.4 Hz, 1H, Im-H1), 8.29 (dd, *J* = 7.6 Hz, *J* = 1.3 Hz, 1H, Pyr-H3 or Pyr-H5), 8.24 (dd, *J* = 7.8 Hz, *J* = 1.3 Hz, 1H, Pyr-H3 or Pyr-H5), 8.14 (dd, *J* = 7.7 Hz, *J* = 7.7 Hz, 1H, Pyr-H4), 7.33 (d, *J* = 1.3 Hz, 1H, Im-H2), 5.02 (dd, *J* = 5.6 Hz, *J* = 8.9 Hz, 1H, CH), 3.52 (ddd, *J* = 15.2 Hz, *J* = 5.6 Hz, *J* = 0.8 Hz, 1H, CH_2-1A), 3.43 (m, 2H, CH_2-2), 3.25 (dd, *J* = 15.7 Hz, *J* = 9.0 Hz, 1H, CH_2-1B), 1.70 (tq, *J* = 7.3 Hz, *J* = 7.3 Hz, 2H, CH_2-3), 1.00 (t, *J* = 7.4 Hz, 3H, CH_3) ppm.

^{13}C NMR (125 MHz, CD_3OD): δ 174.5 (Amide-His), 165.9 and 165.8 (2 Amide-pic), 150.5 (Pyr-C), 149.6 (Pyr-C), 140.5 (Pyr-CH), 135.0 (Im-CH1), 131.6 (Im-C), 126.2 (Pyr-CH), 126.0 (Pyr-CH), 118.3 (Im-CH2), 53.4 (CH), 42.5 (CH_2-2), 28.1 (CH_2-1), 23.9 (CH_2-3), 11.8 (CH_3) ppm.

The chemical shifts were attributed according to HSQC and HMBC spectra.

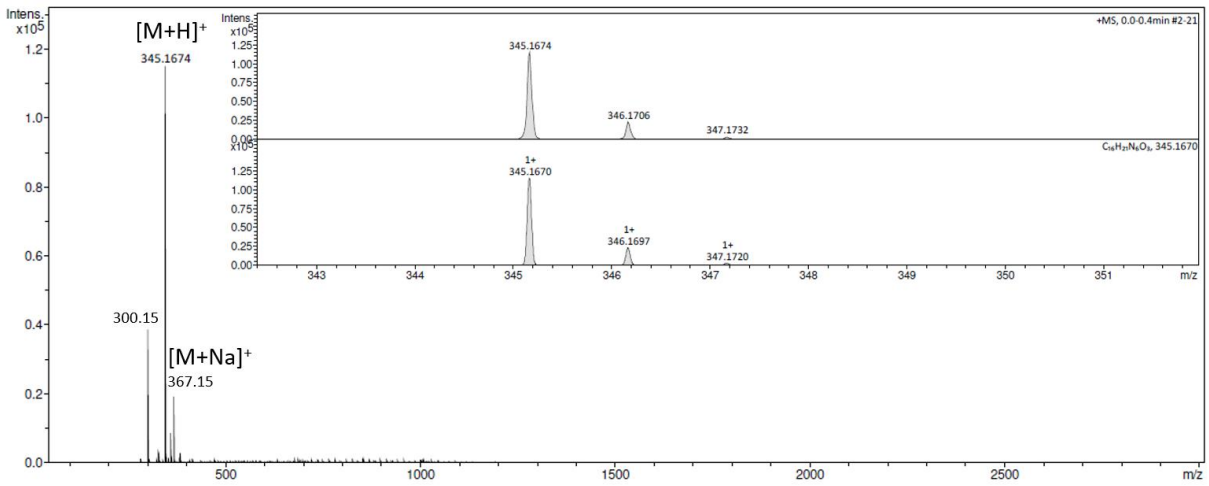

Figure S10: HR-ESI-MS spectrum of C3AmpicH.

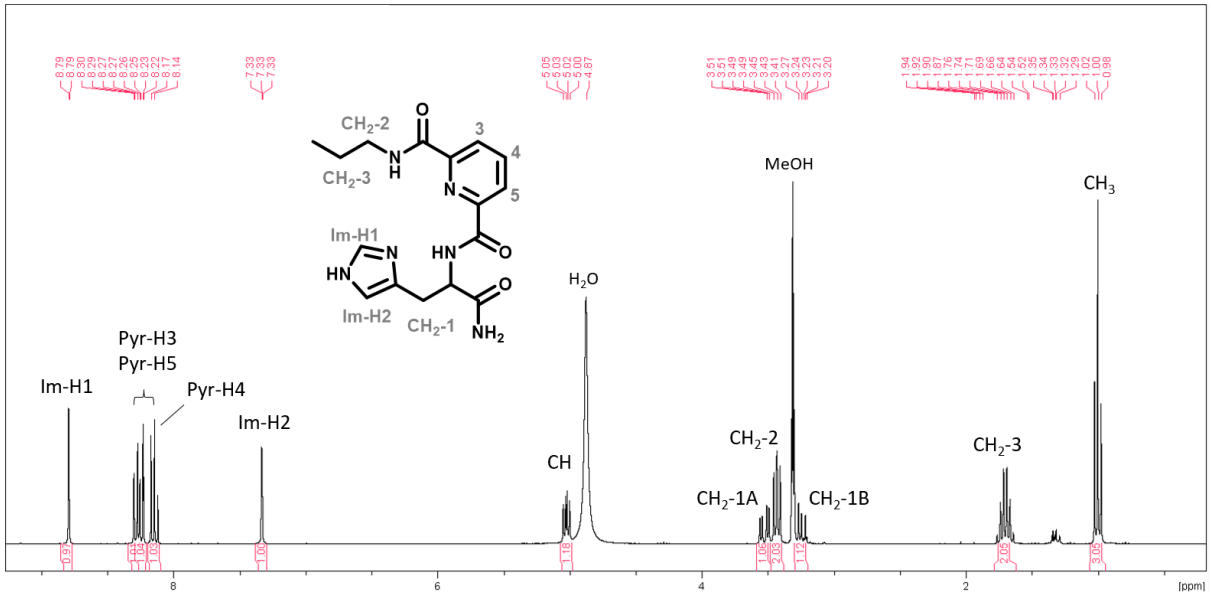

Figure S11: ^{1}H-NMR spectrum of C3AmpicH (300 MHz, CD_3OD).

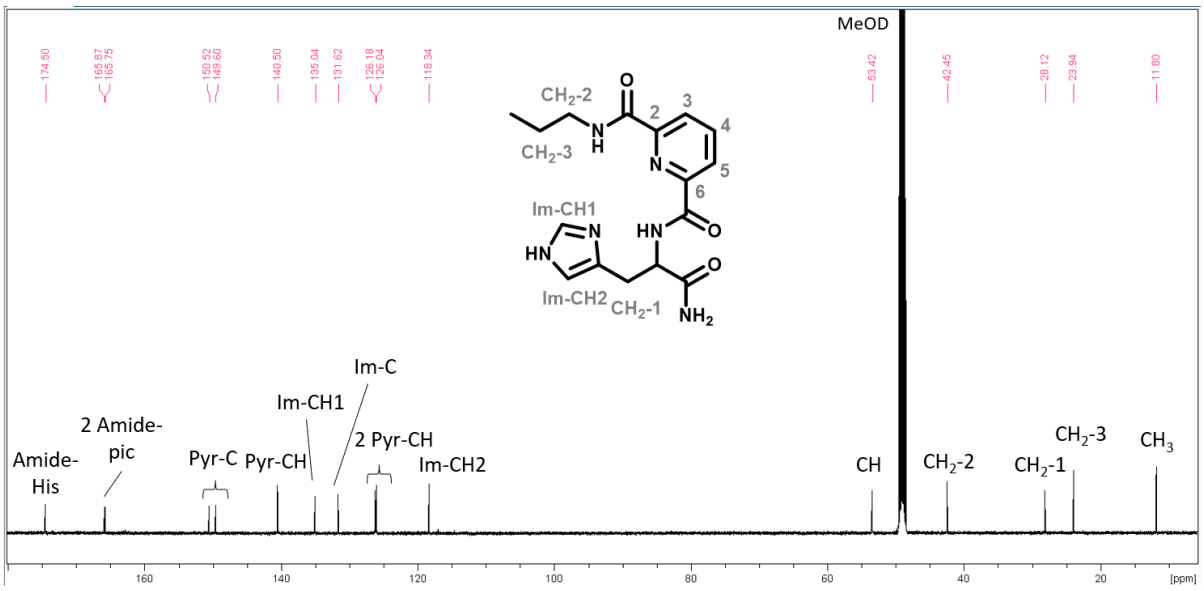

Figure S12: ^{13}C-NMR spectrum of C3AmpicH (125 MHz, CD_3OD).

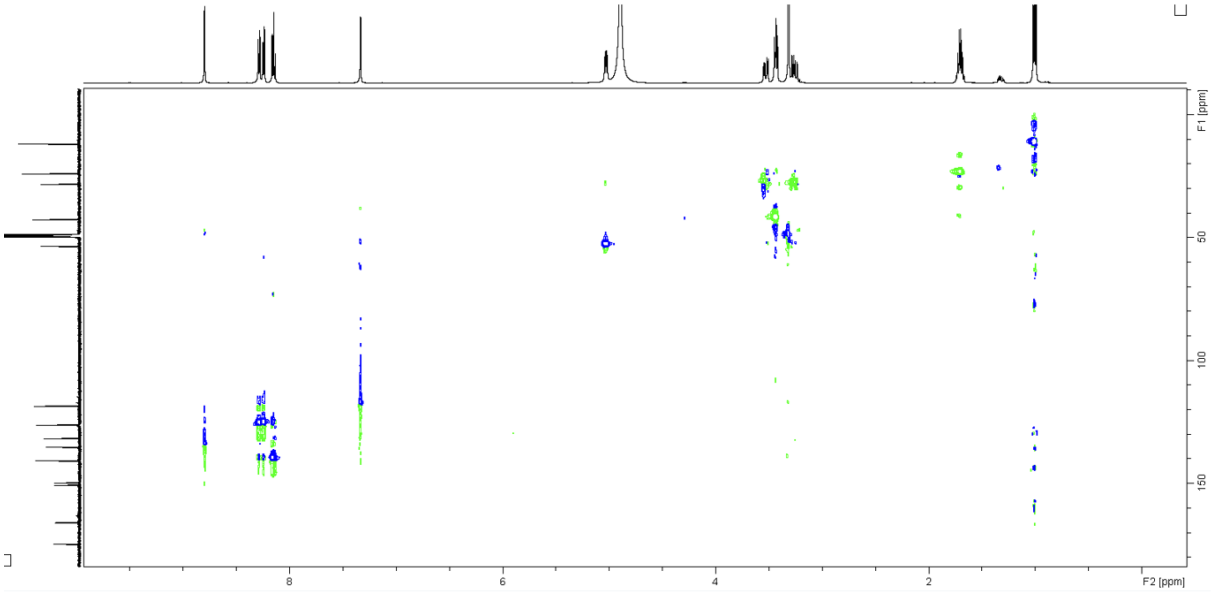

Figure S13: HSQC spectrum of C3AmpicH (500/125 MHz, CD_3OD).

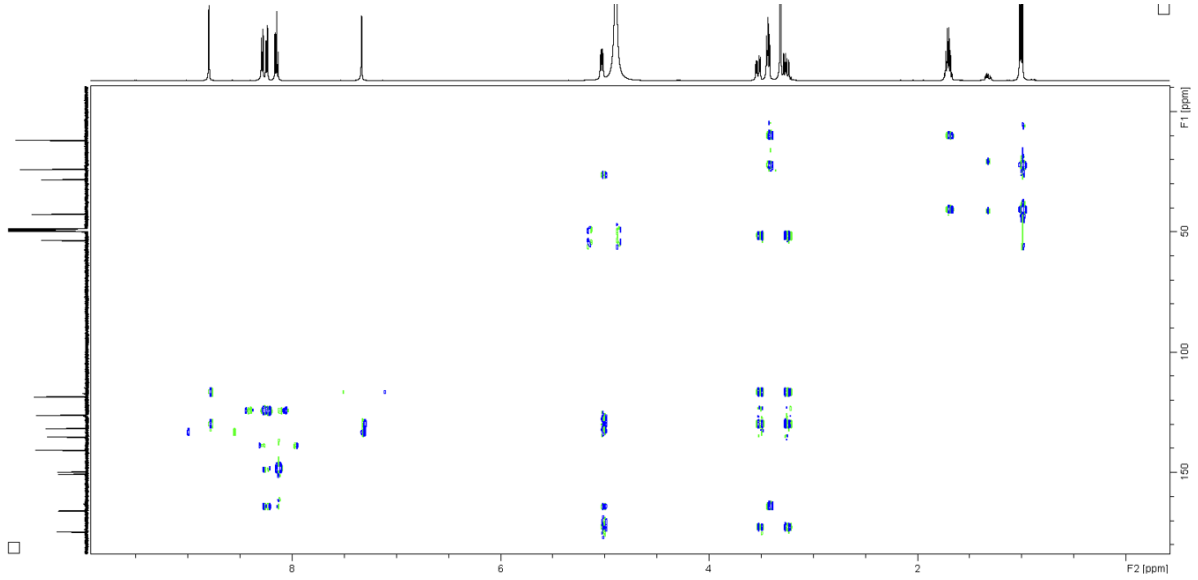

Figure S14: HMBC spectrum of C3AmpicH (500/125 MHz, CD_3OD).

2. Characterization

2.1 Materials and Methods

Preparation of stock solutions:
Stock solutions of the buffers HEPES (500 mM, pH 7.4), TRIS (1 M, pH 7.4), CHES (500 mM, pH 10.0), of citric acid (200 mM), of the metal salts $CuCl_2$ (80 mM), $ZnSO_4$ (100 mM), $Fe(NO_3)_3$, $MnCl_2$, $CaCl_2$, $MgSO_4$ were prepared in Milli-Q water and further diluted for the different experiments. The pH of the buffers was adjusted using NaOH and HCl solutions. The concentration of the $CuCl_2$ stock solution (80 mM) was verified by UV−Vis spectroscopy considering the absorbance of the Cu^{II} d−d band at 780 nm (ε = 12 $M^{-1}cm^{-1}$) in water. The stock solutions of the Cu^{II}-ligands DO3A-C3AmpicH (6.3 mM), C3AmpicH (9.5 mM), HSA (concentration of the ATCUN motif, 665 µM), $aSyn_{46-50}$ (2.3 mM) and $A\beta_{1-16}$ were prepared in Milli-Q water and their concentration were determined by spectrophotometric titration with $CuCl_2$ in HEPES buffer (0.05 M, pH 7.4).

UV-Vis absorption spectra were recorded using 1 cm path length quartz cuvettes (either 100 µL or 1 mL) on a Cary 60 spectrophotometer, which was equipped with either a single cell or a multicell holder. The experiments were conducted at room temperature.

Circular dichroism (CD) spectra were recorded in a 1 cm path cuvette with a Jasco J-810 spectropolarimeter in the 300-600 nm range using a scanning speed of 50 nm/min and 3 accumulations at room temperature. The spectra were smoothed using the Savitzy-Golay method, and the blank (buffer alone) was subtracted from each sample measurement.

Luminescence emission and excitation experiments were carried out on a FluoroMaX Plus spectrofluorometer (Horiba Scientific) with a 150W CW ozone-free xenon arc lamp and FluorEssence™ software in 100 µL or 500 µL quartz cuvettes (1 cm pathway length) at room temperature.

***q* number determination:** The number of lanthanide-bound water molecules, *q,* has been determined by measuring the fluorescence lifetime of Eu^{III}-DO3A-C3AmpicH in both water and deuterated water. These measurements were carried out in 500 µL quartz cuvettes (1 cm pathway length) on a Fluorolog FL3-22 (Horiba JobinYvon) fluorimeter with a pulsed Xe lamp. After the measurement in water, this solvent was lyophilized and the same measurement was carried out in D_2O. The exponential fits of the luminescence decays have been obtained with the program DAS-6, Horiba.

Electron paramagnetic resonance (EPR) spectroscopy: Continuous-wave EPR spectra were recorded on an EMX-plus (Bruker Biospin GmbH, Germany) X-band EPR spectrometer equipped with a high sensitivity resonator (4119HS-W1, Bruker). The g factor was calibrated in experimental conditions using the Bruker strong pitch (g = 2.0028). The spectrometer was operated at *ca*. 9.3 GHz. The principal experimental parameters were: microwave power 0.1 mW; modulation amplitude 5 G; conversion time ca. 200 / 327 ms; time constant ca. 81 ms. 150 mT were swept in ca. 5 min. 4 scans were accumulated to achieve a reasonable Signal to Noise (S/N) ratio. Both samples were supplemented by 10% v/v glycerol to ensure homogeneous protein distributions. Then, samples (*ca.* 50 µL) were introduced to 4 mm outer diameter quartz tubes (Wilmad-Labglass) and freeze-quenched into liquid nitrogen prior to their introduction into the precooled cavity (100 K, achieved by continuous flow liquid nitrogen cryostat). Experimental EPR spectra were best-simulated using labmade routines based on Easyspin toolbox under Matlab (Mathworks) environment where H strain parameter was used to account for experimental line broadening (see Stoll *et al*.).[2]

Relaxometric measurements: Proton relaxation rate ($1/T_1$) measurements as a function of Cu^{2+} addition were performed at 25 °C and 60 MHz on the minispec Brucker "mqvar" relaxometer. The temperature was monitored by a Julabo CD-200F temperature control unit. T_1 were measured with an inversion recovery sequence, and at least 3 reproducible measurements were performed. The experimental errors are ± 5%.
NMRD profiles were recorded at 1.68 mM in Hepes buffer (0.1 M, pH 7.3) on a Stelar SMARTracer fast field cycling relaxometer (0.01-10 MHz) and a Bruker WP80 NMR electromagnet adapted to variable field measurements (20-80 MHz) and controlled by a SMARTracer PC-NMR console. The temperature was monitored by a VTC91 temperature control unit and maintained by a gas flow. The temperature was determined by previous calibration with a Pt resistance temperature probe. At 400 MHz, $1/T1$ measurements were performed in a capillary tube placed in a 5 mm tube containing D2O using the inversion–recovery sequence on a Bruker Avance III (400 MHz) equipped with a 5 mm BBO SmartProbe.The least-squares fit of the ^{1}H NMRD data and simultaneous fit with the ^{17}O NMR data were were analyzed according to the Solomon-Bloembergen-Morgan theory of paramagnetic relaxation (see ESI†). The least-squares fitting of the data was performed using Visualizeur/Optimiseur[48] running on a MATLAB 8.3.0 (R2014a) platform.

2.2 *q*-number determination by luminescence spectroscopy

Horrocks equation: $q = 1.11 * \left(\frac{1}{\tau_{H2O}} - \frac{1}{\tau_{D2O}} - 0.31 - 0.075 * n_{\text{amide bound}}\right)$

Table S1: Luminescence lifetimes and calculated hydration numbers of Eu^{III}-DO3A-AmpicH. Conditions: 500 µM Eu^{III}-DO3A-C3AmpicH in 50 mM HEPES buffer pH 7.4. Excitation at 277 nm. For the calculation of *q*= 0.1 the contribution of the amide bound to the lanthanide ion was considered in the equation.

		Eu^{III}-DO3A-C3AmpicH
τ [ms]	D_2O	1.71
	H_2O	0.41 0.98
q		**1.7** **0.1**

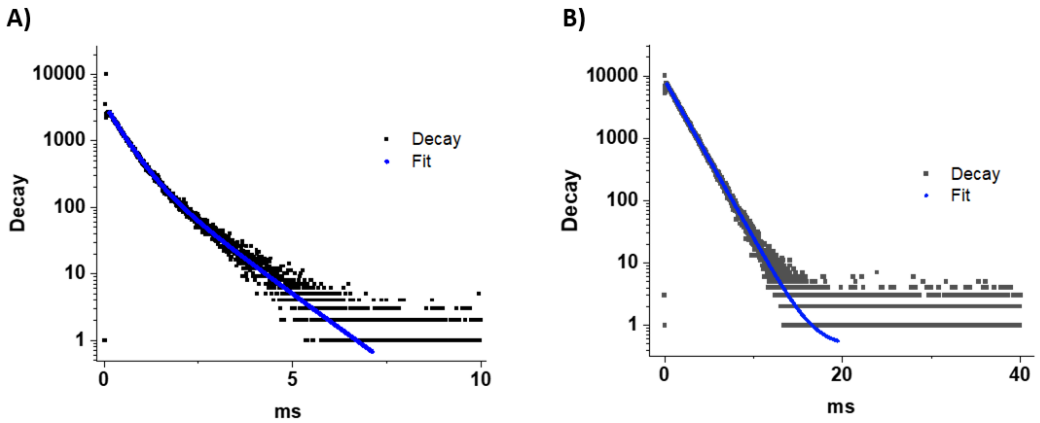

Figure S15: Luminescence decays and fits of Eu^{III}-DO3A-C3AmpicH in water (**A**) and deuterated water (**B**). λ_{ex}= 277 nm, λ_{em}= 615 nm **A)** bi-exponential fit, $t_{1/2}$: 0.409 ms (59%) and 0.984 ms (41%), CHISQ = 0.98, **B)** mono-exponential fit, $t_{1/2}$: 1.71 ms, CHISQ = 0.99. The fits have been obtained in the program DAS-6, Horiba.

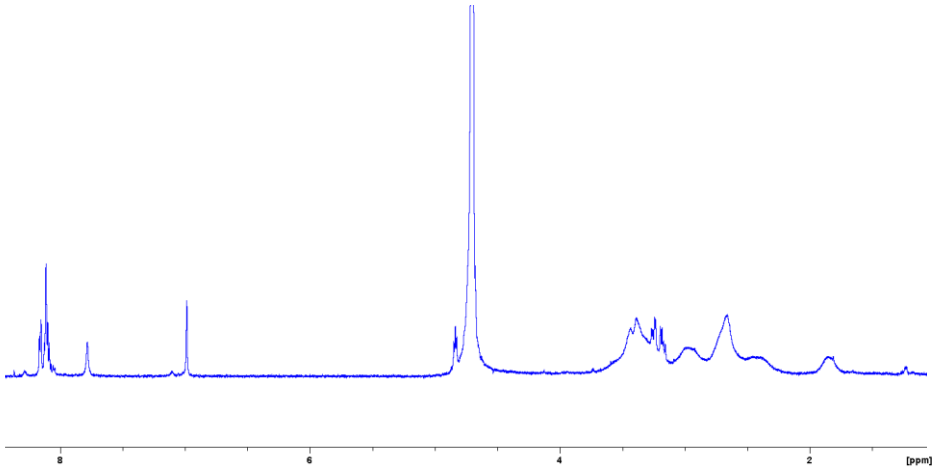

Figure S16: ^1H NMR spectra of Y^{III}-DO3A-C3AmpicH (2.5 mM), in D_2O, pD = 6.8, 25°C, 600 MHz.

Table S2. Best-fit parameters obtained from the fitting of the ^{1}H NMRD profiles to the SBM theory.[3]

Parameters	Gd-DO3A-C3AmpicH	Gd-Cu-DO3A-pyrGH
q^a	1.9	2
k_{ex}^{298} (10^6 s^{-1})^a	11	11
$\Delta H^{\neq}$ (kJ mol^{-1})^a	33.6	33.6
E_R (kJ mol^{-1})	17 ± 2	18
τ_R^{298} (ps)	122 ± 2	99
E_{DGH} (kJ mol^{-1})^a	41 ± 5	55[a]
E_V (kJ mol^{-1})^a	1	1
τ_V^{298} (ps)	25 ± 2	35
Δ^2 (10^{20} s^{-2})	0.55 ± 0.05	0.9

^{a} Fixed during the fitting procedure.

Table S3: Principal EPR parameters obtained through simulations of the EPR experimental spectra obtained with labmade scripts built with Easyspin© toolbox (Mathworks©)[2] g strain parameters were used to account for experimental line broadening. $g_{///}/A_{//}$ ratio is given as a rough estimate of coordination for square-pyramidal Cu^{II} -geometry. While values of 110–120 are characteristic of planar complexes, 130–150 is typical of slight to moderate distortion.[4]

Sample	pH	$g_{\|\|}$ ±0.005	$A_{\|\|}$ (MHz)	$A_{\|\|}$ ($x10^{-4}$ cm^{-1})	$g_{\|\|}/A_{\|\|}$ (cm)
Eu^{III}- Cu^{II}-DO3A-C3AmpicH	7	2.225	510	1.70E-02	131
	9.4	2.206	573	1.91E-02	115
Cu^{II}-C3AmpicH	7.4	2.230	510	1.70E-02	131
	9.5	2.203	590	1.96E-02	112

2.3 Characterization of the Cu^{II} binding

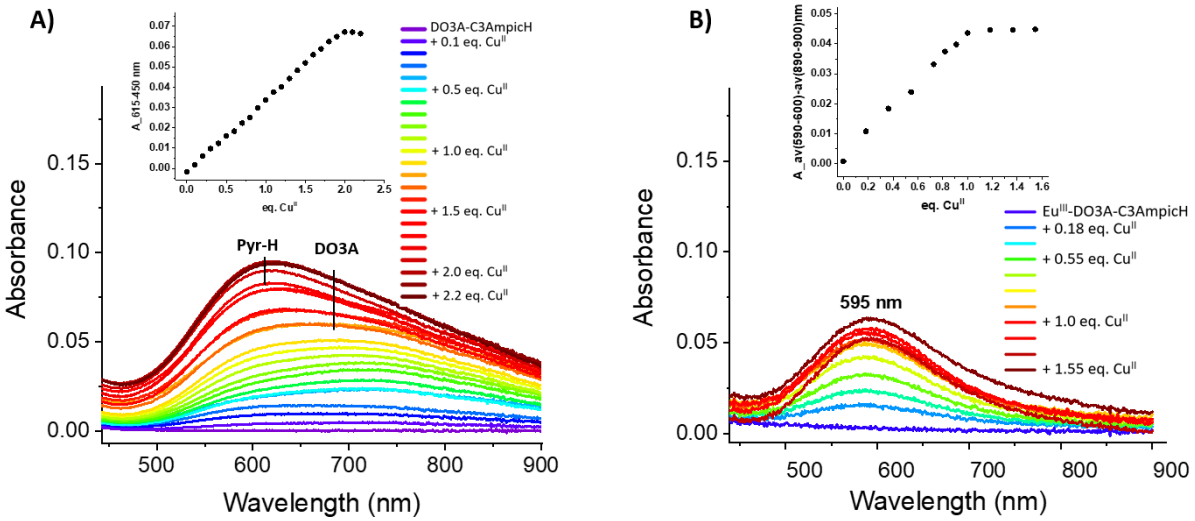

Figure S17: Titration of **A)** DO3A-C3AmpicH and **B)** Eu^{III}-DO3A-C3AmpicH by Cu^{II}. Conditions: **A)** 400 µM DO3A-C3AmpicH, 20 mM HEPES pH 7.4, addition of 0.1 eq. Cu^{II} per step. To monitor the evolution of the d-d band the absorbance at 615 nm has been corrected by the absorbance at 450 nm. Cu^{II} binds in 2 binding sites: DO3A and the C3AmpicH site. Saturation is reached at 2.0 eq of $CuCl_2$, confirming the expected 1:1 binding stoichiometry in both sites. **B)** 440 µM Eu^{III}-DO3A-C3AmpicH, 50 mM HEPES pH 7.4, addition of 0.18 eq. Cu^{II} per step. To monitor the evolution of the d-d band the average absorbance between 590-600 nm has been corrected by the average absorbance between 890-900 nm. A molar absorption coefficient of 114 $M^{-1}\cdot cm^{-1}$ was calculated.

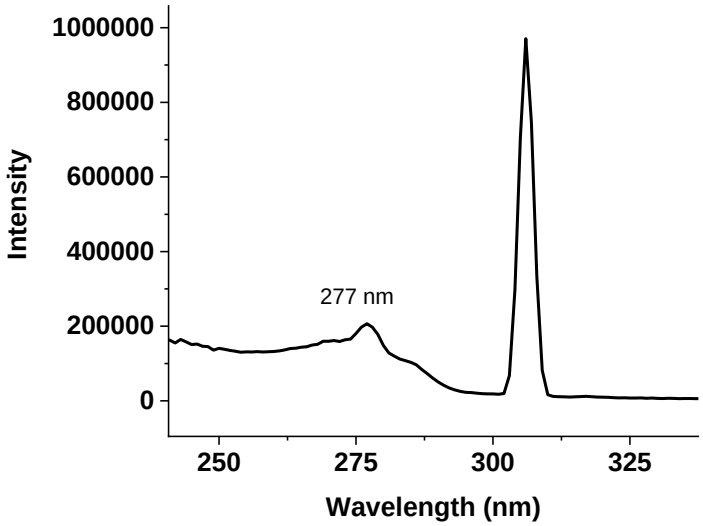

Figure S18: Excitation spectrum of Eu^{III}-DO3A-C3AmpicH. Conditions: 40 µM Eu^{III}-DO3A-C3-AmpicH, 25 mM HEPES pH 7.4, λ_{em} = 613 nm. The signal at 306.5 nm corresponds to the harmonic of the emission wavelength.

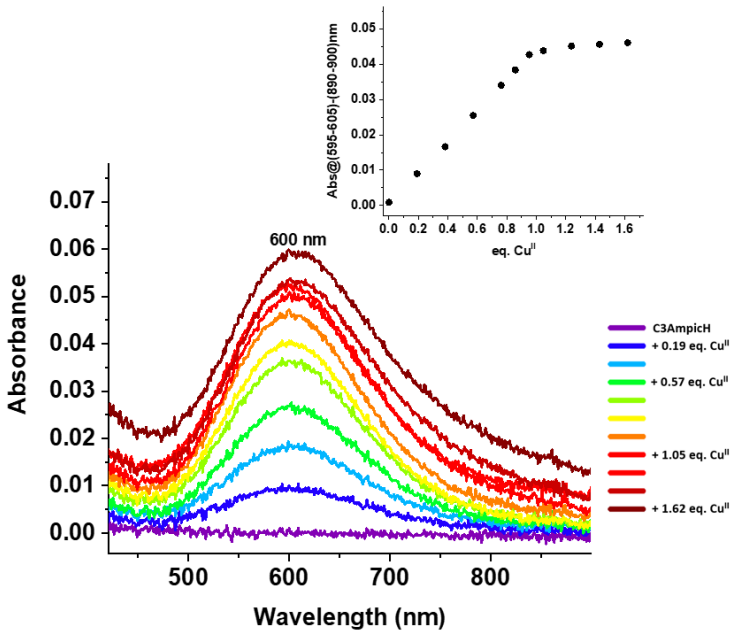

Figure S19: Titration of C3AmpicH with Cu^{II}. Conditions: 420 µM C3AmpicH, 100 mM HEPES pH 7.4 (4 repetitions). To monitor the evolution of the d-d band, the average absorbance between 595-605 nm has been corrected by the average absorbance between 890-900 nm. The maximum absorbance of the d-d band of Cu^{II}-DO3A-C3AmpicH is at 600 nm and the molar absorption coefficient is 112 $M^{-1}\cdot cm^{-1}$.

2.4. pH dependent Cu^{II}-coordination

The influence of the pH on the Cu^{II} coordination of Eu^{III}-C3AmpicH and C3AmpicH has been evaluated by UV-Vis absorption spectroscopy and EPR. For both compounds a blueshift of the absorbance maximum of the d-d band of around 50 nm has been observed upon basification in UV-Vis absorption spectroscopy. (ca. 630 → 580 nm). The results suggest that above pH 8 a 4N Cu^{II}-coordination is predominant, whereas at pH-values below 6 it is a 3N1O-coordination.

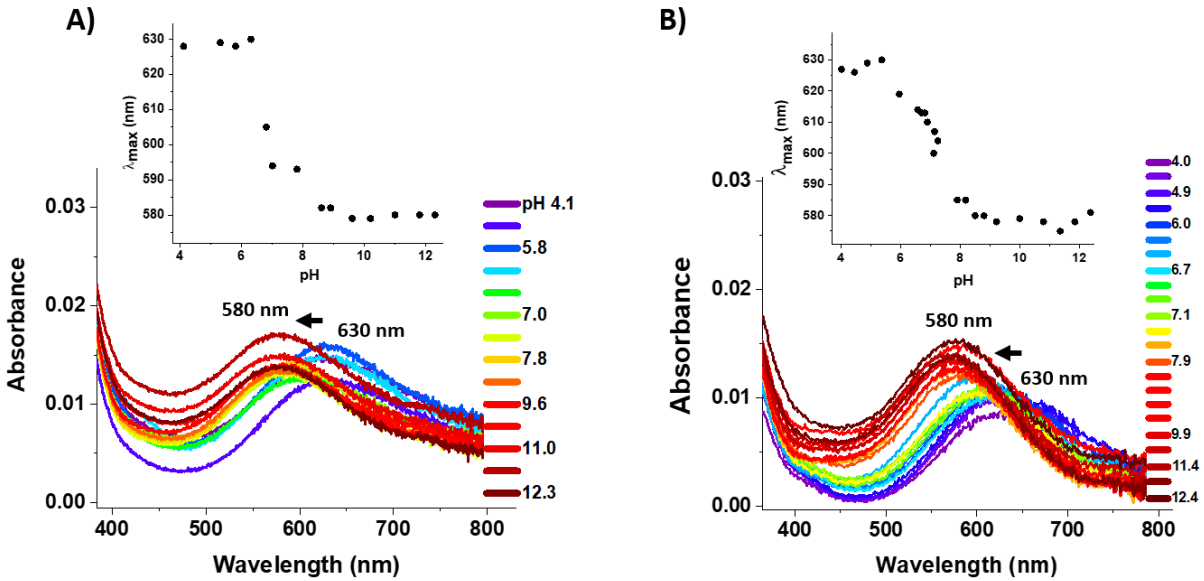

Figure S20: pH-dependence of the Cu^{II}-binding to **A)** Eu^{III}-C3AmpicH and **B)** C3AmpicH. Conditions: 100 µM ligand, 90 µM $CuCl_2$, addition of aqueous NaOH solution. The scatter plot shows the shift of the absorbance maximum according to the pH-value.

EPR experiments were carried out to compare the Cu^{II}-coordination sphere at neutral and basic conditions (pH 7-7.4 and 9.4-9.5). The results suggest a 4N Cu^{II}-coordination sphere at pH 9.4-9.5 where the global charge of the molecule is 0 and a 3N1O Cu^{II}-coordination sphere at neutral pH (+1 charged complex). The discrepancy between the EPR data, which suggests a predominant 3N1O coordination at pH 7–7.4, and the UV-Vis data, which indicates a 4N coordination at the same pH, can be attributed to the different temperatures at which these measurements were conducted.

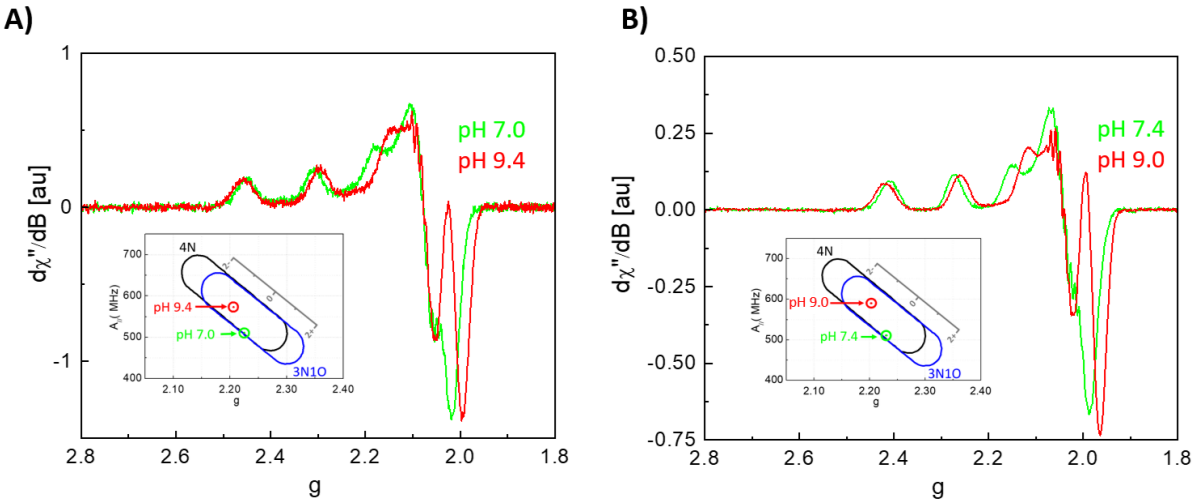

Figure S21: EPR Spectra of **A)** Eu^{III}-Cu^{II}-DO3A-C3AmpicH at pH 7 (green spectrum) and 9.4 (red spectrum) with [Cu^{II}] = 500 μM, [Eu^{III}-DO3A-C3AmpicH] = 600 μM, in 75 mM HEPES or CHES buffer for neutral and basic conditions, respectively and **B)** Cu^{II}-C3AmpicH at pH 7.4 (green spectrum) and 9.5 (red spectrum) with [Cu^{II}] = 500 μM, [C3AmpicH] = 600 μM, in 75 mM HEPES or CHES buffer for neutral and basic conditions, respectively. The samples have been supplemented with 10% glycerol and measured at 100K. Insets: Schematic representations of so-called Peisach-Blumberg diagrams pointing to the complex coordination sphere regarding the $A_{//}$ and $g_{//}$ together with the overall charge of the molecule (see Peisach J. and Blumberg).[5]

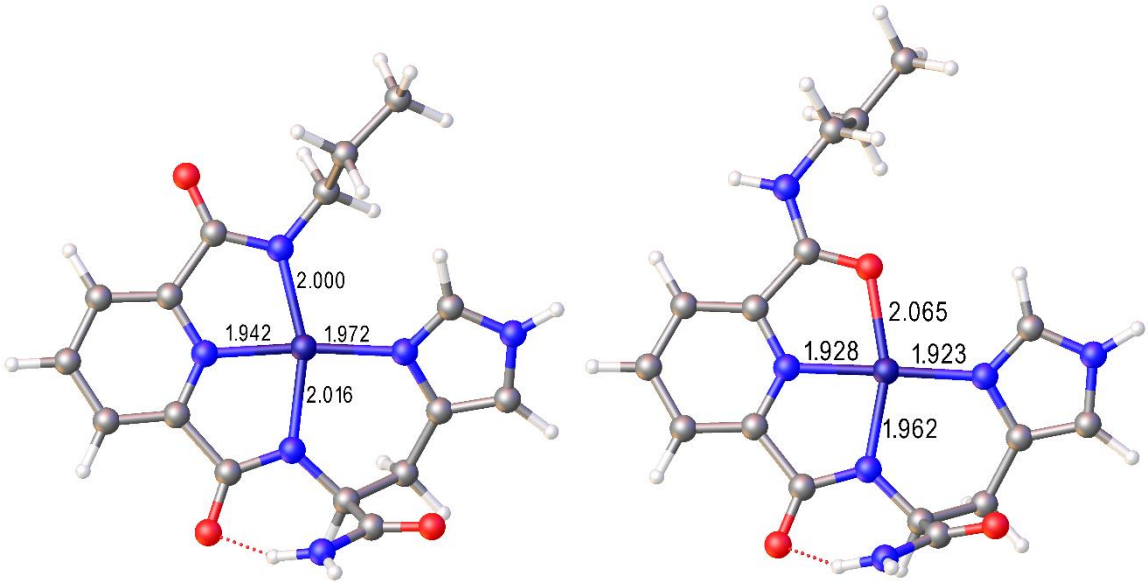

Figure S22: DFT structures calculated for the 4N (left) and 3N1O (right) forms of the Cu^{II}-C3AmpicH complex.

2.5 Competition experiments

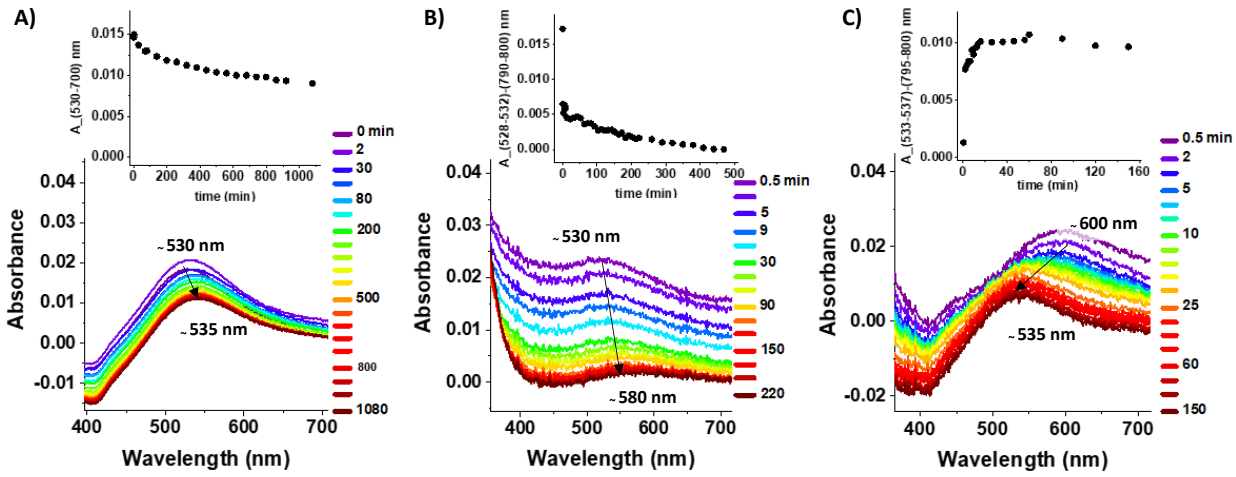

Figure S23: Competition experiments between Eu^{III}-DO3A-C3AmpicH and HSA for Cu^{II} monitored by UV-Vis absorption spectroscopy. **A)** Cu^{II}-HSA + Eu^{III}-DO3A-C3AmpicH (1:1), **B)** Cu^{II}-HSA + Eu^{III}-DO3A-C3AmpicH (1:10), **C)** HSA + Eu^{III}-Cu^{II}-DO3A-C3AmpicH (1:1) Conditions: **A)** 200 µM Eu^{III}-DO3A-C3AmpicH, 200 µM HSA, 180 µM $CuCl_2$, 50 mM HEPES pH 7.4. **B)** 500 µM Eu^{III}-DO3A-C3AmpicH, 50 µM HSA, 45 µM $CuCl_2$, 50 mM HEPES pH 7.4 **C)** 200 µM Eu^{III}-DO3A-C3AmpicH, 200 µM HSA, 180 µM $CuCl_2$, 50 mM HEPES pH 7.4.
When Eu^{III}-DO3A-C3AmpicH is added in a tenfold excess relative to HSA, the shift of the d-d band becomes more pronounced, approximately 50 nm, indicating a greater retrieval of copper from HSA.

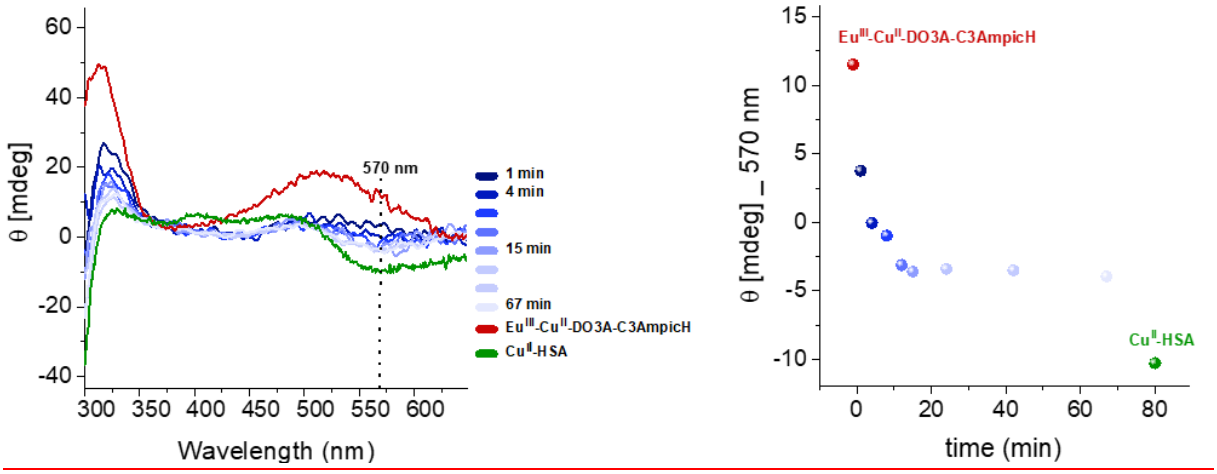

Figure S24: Competition experiment between HSA and Eu^{III}-DO3A-C3AmpicH for Cu^{II} monitored by CD. Cu^{II} transfer from Eu^{III}-Cu^{II}-DO3A-C3AmpicH to HSA. Conditions: 500 µM Eu^{III}-DO3A-C3AmpicH, 500 µM HSA, 450 µM $CuCl_2$, 50 mM HEPES pH 7.4. The curves were smoothed using the Savitzky Golay 15 filter.

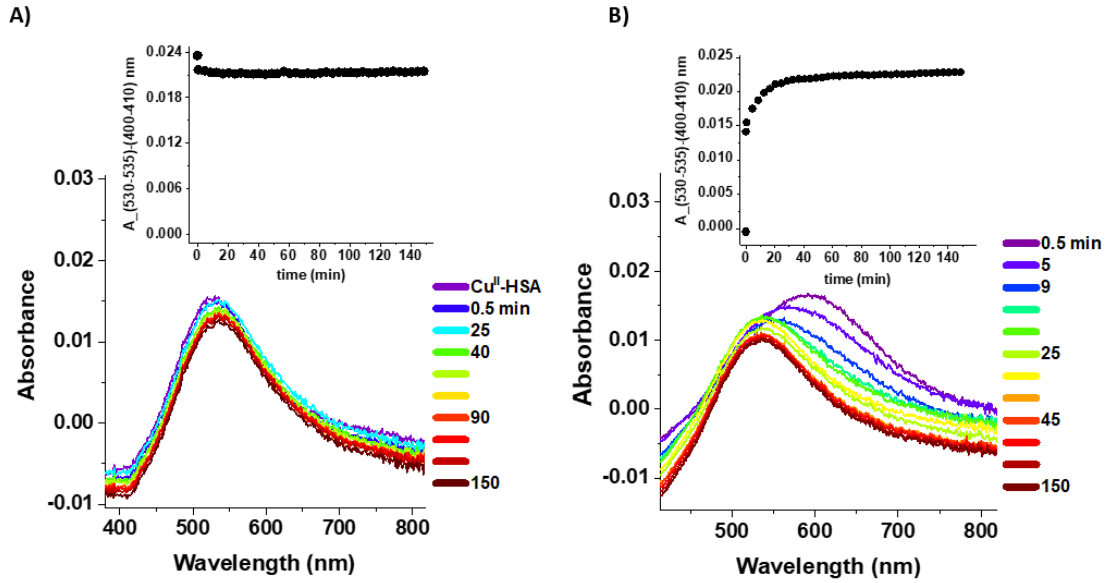

Figure S25: UV-Vis absorption spectra of the competition reaction between **A)** Cu^{II}-HSA and C3AmpicH and **B)** HSA and Cu^{II}-C3AmpicH. Conditions: 200 µM HSA, 200 µM C3AmpicH, 180 µM $CuCl_2$, 50 mM HEPES pH 7.4 (duplicate).

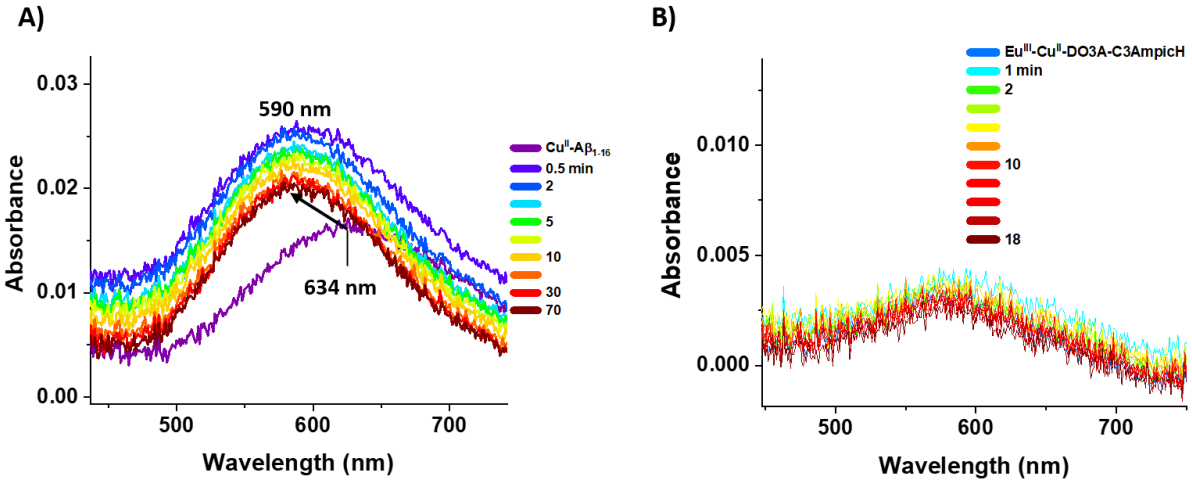

Figure S26: Competition experiments with $A\beta_{1-16}$ (log K_{app} = 10^{10}). **A)** Competition between Cu^{II}-$A\beta_{1-16}$ and Eu^{III}-DO3A-C3AmpicH (1:1). Conditions: 200 µM Eu^{III}-DO3A-C3AmpicH, 180 µM $CuCl_2$, 200 µM $A\beta_{1-16}$, 50 mM HEPES pH 7.4. Eu^{III}-DO3A-C3AmpicH immediately retrieves Cu^{II} bound to $A\beta_{1-16}$. **B)** Competition between $A\beta_{1-16}$ and Eu^{III}-Cu^{II}-DO3A-C3AmpicH (1:1). Conditions: 30 µM Eu^{III}-DO3A-C3AmpicH, 27 µM $CuCl_2$, 300 µM $A\beta_{1-16}$, 50 mM HEPES pH 7.4, $A\beta_{1-16}$ does not retrieve Cu^{II} from Eu^{III}-DO3A-C3AmpicH, not even in 10-fold excess.

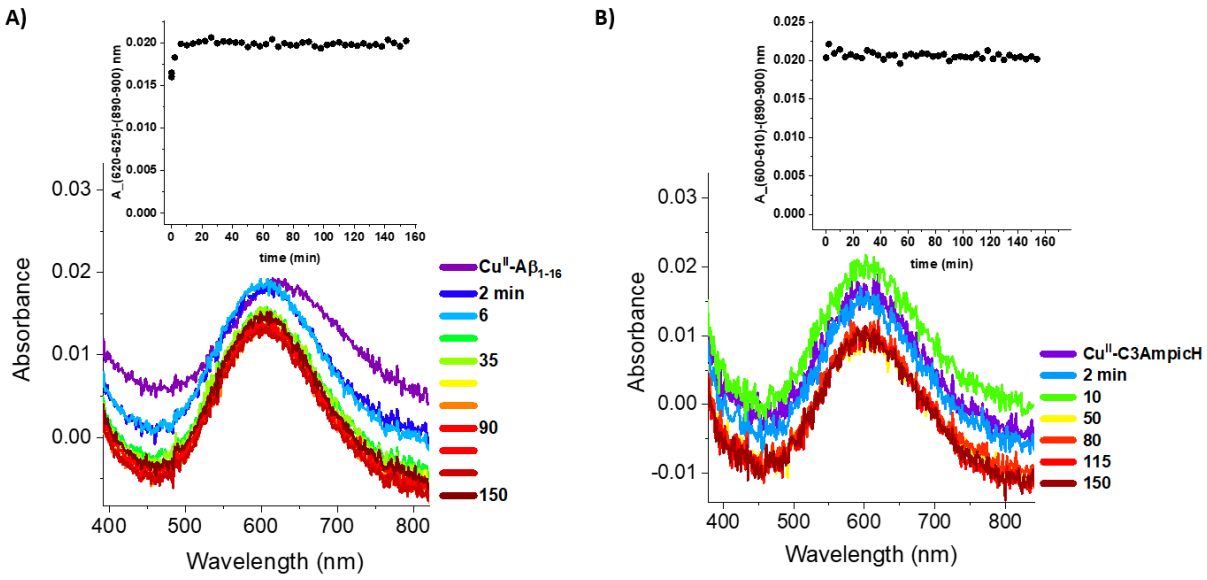

Figure S27: UV-Vis spectra of the competition reaction between **A)** Cu^{II}-Aβ$_{1-16}$ and C3AmpicH and **B)** Aβ$_{1-16}$ and Cu^{II}-C3AmpicH. Conditions : 200 µM Aβ$_{1-16}$, 200 µM C3AmpicH, 180 µM $CuCl_2$, 50 mM HEPES pH 7.4 (duplicate).

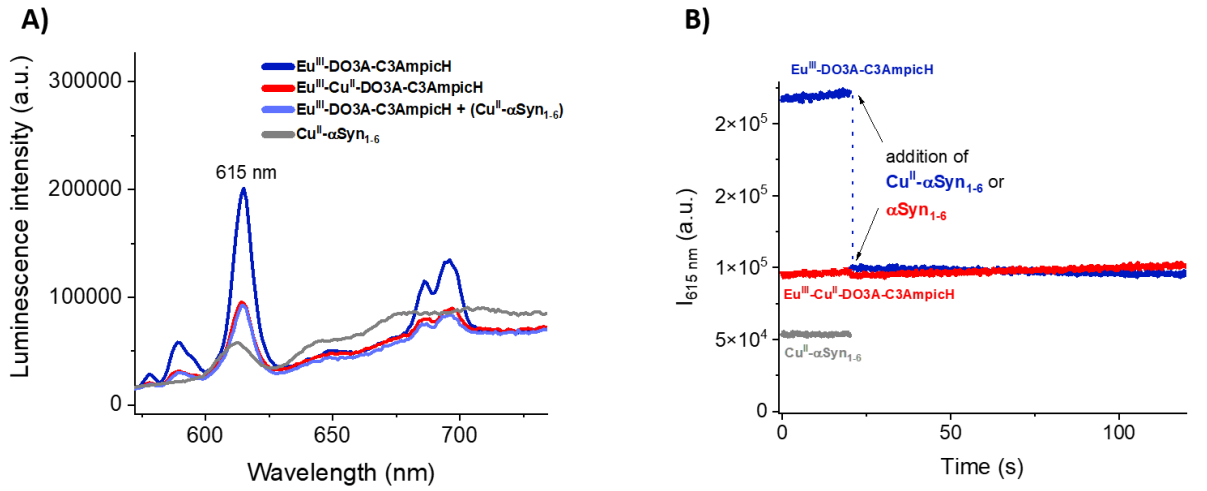

Figure S28: A) Luminescence spectra of the Eu^{III}-sensor with and without copper, of Cu^{II}-αSyn$_{1-6}$ and of the endpoint of the competition reaction**. B)** Evolution of the Eu^{III}-luminescence emission intensity at 615 nm. Conditions : 40 µM Eu-DO3A-C3AmpicH, 40 µM αSyn$_{1-6}$, 36 µM $CuCl_2$, 25 mM HEPES pH 7.4, λ_{ex}=277 nm. The small remaining luminescence intensity observed at 615 nm for the Cu^{II}-α-Syn control is attributed to a background signal, which is also present at the same intensity in the HEPES buffer alone. This signal shifts with changes in the excitation wavelength and is likely due to Raman scattering.

2.6 Selectivity over other metal ions

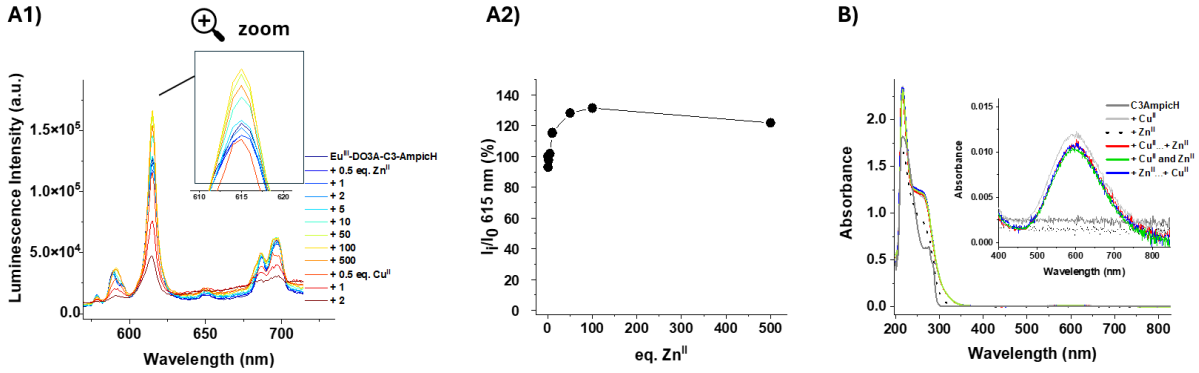

Figure S29: A1) Luminescence emission spectra of the titration of Eu^{III}-DO3A-C3AmpicH with Zn^{II}. **A2)** Evolution of the luminescence emission intensity at 615 nm. Conditions: 40 µM Eu^{III}- DO3A-C3AmpicH, 100 mM HEPES pH 7.4, λ_{exc} = 277 nm. **B)** UV-Vis spectrum of the addition of 1 eq. Cu^{II} and 10 eq. Zn^{II} to C3AmpicH. Conditions: 100 µM C3AmpicH, 100 µM $CuCl_2$, 1 mM $ZnSO_4$, 10 mM TRIS buffer pH 7.4.

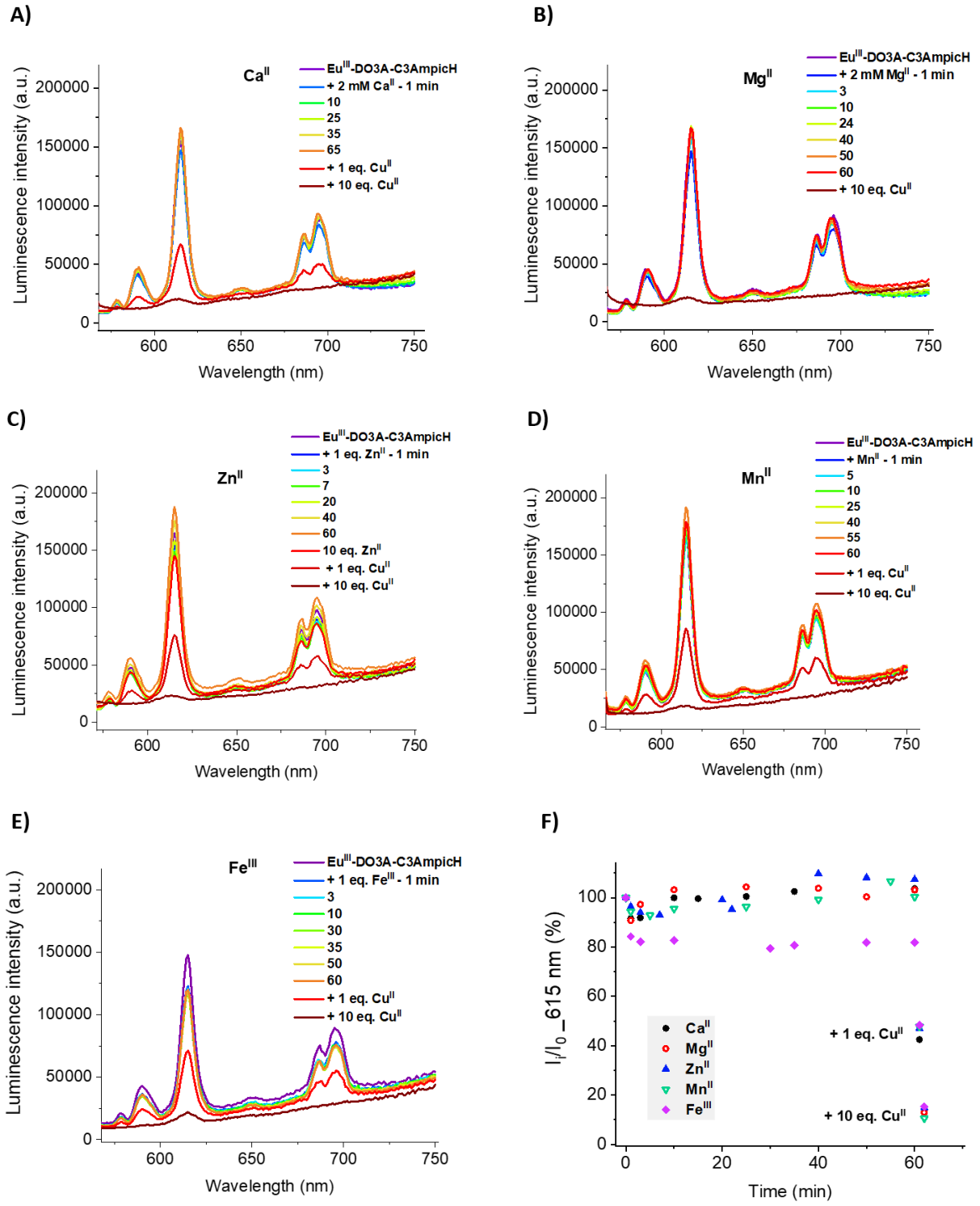

Figure S30: Luminescence emission spectra of Eu^{III}-DO3A-C3AmpicH upon the separate addition of physiological metal ions (A-E) and scatter plot of the evolution of the relative luminescence intensity at 615 nm over time (F). Conditions: 40 µM Eu^{III}-DO3A-C3AmpicH, 100 mM HEPES pH 7.4, addition of 2 mM $MgSO_4$ or 2 mM $CaCl_2$ or 40 µM $Fe(NO_3)_3$ + 2 mM citric acid or 40 µM $ZnSO_4$ or 40 µM $MnCl_2$,. λ_{exc} = 277 nm.

As Fe^{III} is very strongly bound to transferrin with a log $K_{a(pH7.4)}$ = 22 and there is more apo- than holo-transferrin, this ion is however not expected to interfere with the copper binding in a physiological context.[6]

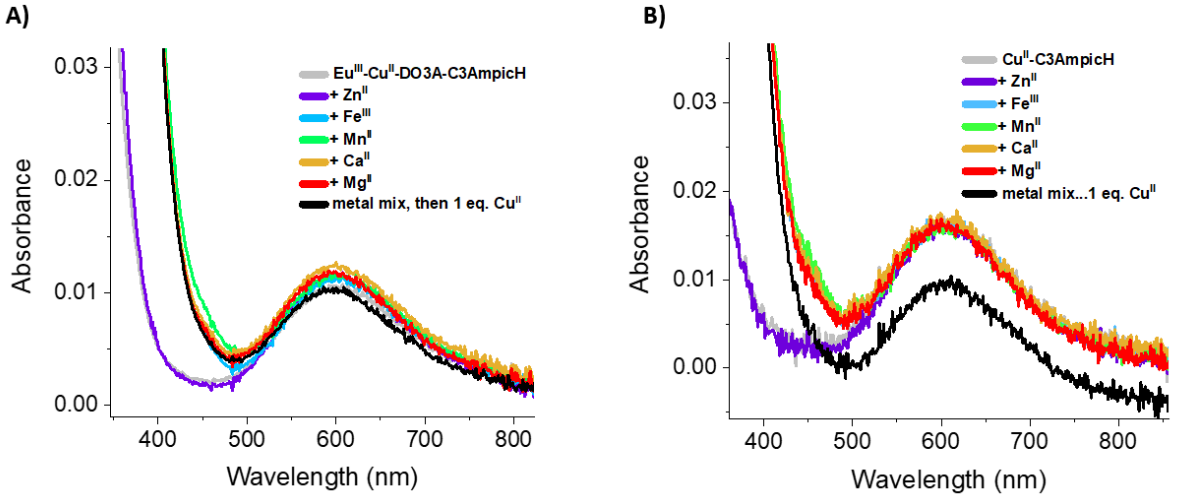

Figure S31: Addition of metal ions to the preformed **A)** Eu^{III}-Cu^{II}-DO3A-C3AmpicH complex and **B)** Cu^{II}-C3AmpicH. Conditions: A) 150 µM Eu^{III}-DO3A-C3AmpicH, 100 µM $CuCl_2$, 100 µM $ZnSO_4$, 100 µM $Fe(NO_3)_3$, 100 µM $MnCl_2$, 2 mM $CaCl_2$, 2 mM $MgSO_4$, 100 mM HEPES pH 7.4, 2 mM citric acid. B) 150 µM C3AmpicH, 150 µM $CuCl_2$, 150 µM $ZnSO_4$, 150 µM $Fe(NO_3)_3$, 150 µM $MnCl_2$, 2 mM $CaCl_2$, 2 mM $MgSO_4$, 150 mM HEPES pH 7.4, 2 mM citric acid. (duplicate).

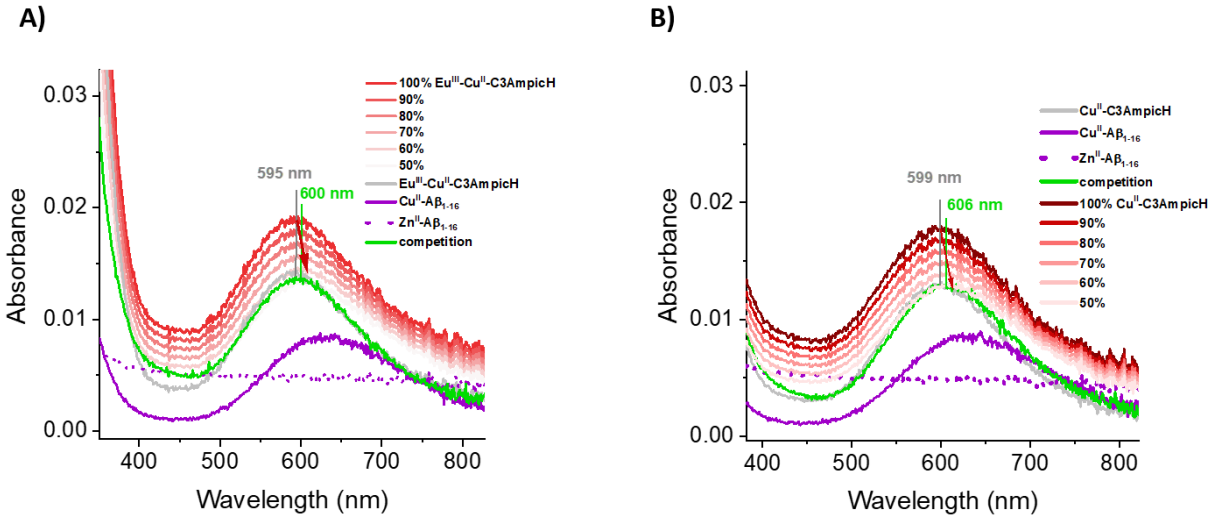

Figure S32: UV-VIS spectra of the selectivity experiments involving **A)** Eu^{III}-DO3A-C3AmpicH or **B)** C3-AmpicH and $A\beta_{1-16}$, Cu^{II} and Zn^{II} in an equimolar ratio. Conditions: A) 100 µM C3AmpicH, 100 µM $A\beta_{1-16}$, 100 µM $CuCl_2$, 100 µM $ZnSO_4$ in 10 mM TRIS buffer pH 7.4. B) 100 µM Eu^{III}-DO3A-C3AmpicH, 100 µM $A\beta_{1-16}$, 100 µM $CuCl_2$, 100 µM $ZnSO_4$, 10 mM TRIS pH 7.4. The red curves were obtained as a linear combination of the curves of Cu^{II}-C3AmpicH *or* Eu^{III}-Cu^{II}-DO3A-C3AmpicH, Cu^{II}-$A\beta_{1-16}$ and Zn^{II}-$A\beta_{1-16}$ using different coefficients. The linear combination abbreviated with 90% for example results from the addition of 0.9*Eu^{III}-Cu^{II}-DO3A-C3AmpicH + 0.1* Cu^{II}-$A\beta_{1-16}$ + 0.9* Zn^{II}-$A\beta_{1-16}$. The spectra of Eu^{III}-Zn^{II}-DO3A-C3AmpicH and Zn^{II}-C3AmpicH have not been considered in these calculation as they do not show any absorbance in the studied wavelength range. The comparison of the absorbance maximum of these linear combinations with the one of the competition experiments, suggests that around 80-90% of the copper seem to be bound to the ligand and 10-20% to $A\beta_{1-16}$.

2.7 Equations used for the fitting of the ^{1}H NMRD profiles

The measured longitudinal proton relaxation rate, R_1^{obs} is the sum of the paramagnetic and diamagnetic contributions as expressed in Eq. 1, where r_1 is the proton relaxivity:

$$R_1^{obs} = R_1^d + R_1^p = R_1^d + r_1 \times c_{Gd} \quad [1]$$

The relaxivity can be divided into terms of inner and outer sphere, as follows:

$$r_1 = r_{1is} + r_{1os} \quad [2]$$

The inner sphere term is obtained in Eq. 3, where q is the number of inner sphere water molecules.[7]

$$r_{1is} = \frac{1}{1000} \times \frac{q}{55.55} \times \frac{1}{T_{1m}^H + \tau_m} \quad [3]$$

The longitudinal relaxation rate of inner sphere protons, $1/T_{1m}{}^H$ is expressed by Eq. 4, where r_{GdH} is the effective distance between the electron charge and the ^{1}H nucleus, ω_I is the proton resonance frequency and ω_S is the Larmor frequency of the Gd^{III} electron spin.

$$\frac{1}{T_{1m}^H} = \frac{2}{15}\left(\frac{\mu_0}{4\pi}\right)^2 \frac{\hbar^2 \gamma_I^2 \gamma_S^2}{r_{GdH}^6} S(S+1) \times \left[3J(\omega_I;\tau_{d1}) + 7J(\omega_S;\tau_{d2})\right] \quad [4]$$

$$\frac{1}{\tau_{di}} = \frac{1}{\tau_m} + \frac{1}{\tau} + \frac{1}{T_{ie}} \quad [5]$$

The longitudinal and transverse electronic relaxation rates, $1/T_{1e}$ and $1/T_{2e}$ are expressed by Eq. 6-7, where τ_V is the electronic correlation time for the modulation of the zero-field-splitting interaction, E_V the corresponding activation energy and Δ^2 is the mean square zero-field-splitting energy. We assumed a simple exponential dependence of τ_V versus $1/T$.

$$\left(\frac{1}{T_{1e}}\right)^{ZFS} = \frac{1}{25}\Delta^2 \tau_v \left\{4S(S+1) - 3\right\}\left(\frac{1}{1+\omega_S^2\tau_v^2} + \frac{4}{1+4\omega_S^2\tau_v^2}\right) \quad [6]$$

$$\left(\frac{1}{T_{2e}}\right)^{ZFS} = \Delta^2 \tau_v \left(\frac{5.26}{1+0.372\omega_S^2\tau_v^2} + \frac{7.18}{1+1.24\omega_S^2\tau_v^2}\right) \quad [7]$$

$$\tau_v = \tau_v^{298} \, exp\left\{\frac{E_v}{R}\left(\frac{1}{T} - \frac{1}{298.15}\right)\right\} \quad [8]$$

The outer-sphere contribution can be described by Eq. 9 where N_A is the Avogadro constant, and J_{os} is its associated spectral density function.[8,9]

$$r_{1os} = \frac{32 N_A \pi}{405}\left(\frac{\mu_0}{4\pi}\right)^2 \frac{\hbar^2 \gamma_S^2 \gamma_I^2}{a_{GdH} D_{GdH}} S(S+1)\left[3J_{os}(\omega_I, T_{1e}) + 7J_{os}(\omega_S, T_{2e})\right] \qquad [9]$$

$$J_{os}(\omega, T_{je}) = Re\left[\frac{1 + \frac{1}{4}\left(i\omega\tau_{GdH} + \frac{\tau_{GdH}}{T_{je}}\right)^{1/2}}{1 + \left(i\omega\tau_{GdH} + \frac{\tau_{GdH}}{T_{je}}\right)^{1/2} + \frac{4}{9}\left(i\omega\tau_{GdH} + \frac{\tau_{GdH}}{T_{je}}\right) + \frac{1}{9}\left(i\omega\tau_{GdH} + \frac{\tau_{GdH}}{T_{je}}\right)^{3/2}}\right] \qquad j = 1, 2 \qquad [10]$$

The diffusion coefficient for the diffusion of a water proton away from a Gd^{III} complex, D_{GdH}, is assumed to obey an exponential law versus the inverse of the temperature, with an activation energy $E_{GdH,}$ as given in Eq. 11 D_{GdH}^{298} is the diffusion coefficient at 298.15 K.

$$D_{\mathrm{GdH}} = D_{\mathrm{GdH}}^{298} \exp\left\{\frac{E_{\mathrm{GdH}}}{R}\left(\frac{1}{298.15} - \frac{1}{T}\right)\right\} \qquad [11]$$

In the fitting procedure, several parameters were fixed to the common values, such as: the relative diffusion coefficient, set to D_{GdH}^{298} = 2.6 x 10^{-9} m^2 s^{-1} and the activation energy of the modulation of the zero-field splitting, set to E_v = 1 kJ mol^{-1}. The water exchange rate and its activation energy were fixed to the values of Gd-DO3A due to the similar coordination sphere (k_{ex} = 11.10^6 s^{-1}, $\Delta H^{\neq}$ = 33 kJ.mol^{-1}). [10] The diffusion coefficient (D_t) was fixed to 2.6.10^{-9} $m^2.s^{-1}$, the Gd-water proton distance was fixed to the common value of 3.1 Å, while that of closest approach between Gd^{3+} and outer sphere protons to 3.5 Å. The rotational correlation time (τ_R), its activation energy (E_R), the activation energy of the relative diffusion coefficient (E_{DGdH}) and the electronic parameters, i.e. the mean square of the zero-field splitting (Δ^2) and the correlation time for the modulation of the zero-field splitting (τ_v^{298}) were fitted, but these electronic parameters should not be over-interpreted

2.8 DFT calculations

Geometry optimizations and frequency calculations were conducted with the Gaussian16 package (version C.01)[11], using the wB97XD functional[12], which incorporates empirical dispersion corrections, and the Def2-TZVP basis set[13] for the ligand atoms and Cu. For Gd we used the quasi-relativistic effective core potential of Dolg at al. (53 electrons in the core) and its associated (7s6p5d)/[5s4p3d] basis set. [14] The solvent effects of bulk water were incorporated using the integral equation formalism variant of the polarized continuum model (IEFPCM) implemented in Gaussian16.[15] The Gd complexes were modelled including a few explicit second-sphere water molecules to improve the description of the complexes.[16] The ORCA program package (version 5.0.3)[17,18] was used to calculate the *g*- and *A*-tensors. The *A*-tensors were obtained with the TPSS functional[19], while g-tensors were calculated with the double hybrid PBE0-DH functional.[20] These calculations included scalar relativistic effects using the ZORA approximation[21,22], using the def2-TZVPP basis set recontracted for ZORA calculations for Cu and the ZORA-def2-TZVP for ligand atoms.[13,23] The calculations were accelerated using the resolution of

identity (RI) the resolution of identity and chain-of-spheres (RIJCOSX)[24] approximations for TPSS and PBE0-DH, respectively, with auxiliary basis sets obtained with the Autoaux procedure[25]. All ORCA calculations incorporated water solvent effects with the SMD solvation model.[26] The spin-orbit coupling (SOC) contributions to the hyperfine coupling constant tensor was considered using the spin-orbit mean-field (SOMF(1X)) method.[24,27]

Table S4: Optimized Cartesian coordinates (Å) obtained for the Eu^{III}-DO3A-C3AmpicH system (amide bound) using DFT calculations.[a]

Center Number	Atomic Number	Coordinates X	Y	Z
1	7	-3.193243	-2.460327	-0.120128
2	6	-4.545969	-1.869983	-0.287873
3	6	-4.682183	-0.792369	-1.334920
4	7	-3.966653	0.445566	-1.004063
5	6	-3.938335	1.334732	-2.175923
6	6	-3.014022	0.852993	-3.268711
7	7	-1.625123	0.658398	-2.827047
8	6	-0.959155	-0.274920	-3.748543
9	6	-1.310229	-1.717782	-3.425560
10	7	-0.818729	-2.159336	-2.108019
11	6	-1.438145	-3.438514	-1.711627
12	6	-2.896949	-3.340774	-1.280160
13	6	-4.596045	1.155630	0.118475
14	6	-3.761119	1.196149	1.386219
15	8	-3.953012	2.147399	2.161925
16	8	-2.953150	0.243989	1.579604
17	6	-0.935211	1.948604	-2.741794
18	6	-1.299732	2.713844	-1.473216
19	8	-1.436734	3.936646	-1.496751
20	8	-1.414967	2.008971	-0.412029
21	6	0.646144	-2.284841	-2.153275
22	6	1.398118	-0.997613	-1.821030
23	8	2.586803	-0.934182	-2.146825
24	8	0.757394	-0.090854	-1.211838
25	1	-5.551035	0.695608	0.392450
26	1	-4.830903	2.180347	-0.163045
27	1	-1.127324	2.575039	-3.617801
28	1	0.137838	1.763300	-2.672641
29	1	0.968344	-3.008209	-1.406590
30	1	0.982847	-2.654766	-3.126032
31	1	-4.839376	-1.461314	0.677355
32	1	-5.263039	-2.665976	-0.523275
33	1	-5.752282	-0.590187	-1.472130
34	1	-4.316654	-1.155053	-2.293089
35	1	-4.944573	1.446971	-2.599552
36	1	-3.633502	2.323372	-1.841298
37	1	-3.050915	1.574278	-4.094213
38	1	-3.381873	-0.085013	-3.677050
39	1	-1.245475	-0.070807	-4.786635
40	1	0.115194	-0.120365	-3.690726
41	1	-2.391404	-1.841134	-3.448647
42	1	-0.907212	-2.367667	-4.211271
43	1	-0.836817	-3.840482	-0.902420

44	1	-1.387595	-4.161458	-2.535544
45	1	-3.490106	-2.999052	-2.125996
46	1	-3.245321	-4.357908	-1.070829
47	64	-1.357579	-0.355188	-0.213215
48	8	-1.524996	4.969990	3.106431
49	8	0.054504	0.551156	1.704330
50	1	-2.137283	5.022437	2.349364
51	1	-1.913112	4.297369	3.694116
52	1	-0.329060	0.337277	2.579323
53	1	0.140817	1.524814	1.722685
54	8	-3.102921	4.594290	0.797945
55	1	-3.443993	3.750980	1.133262
56	1	-2.525004	4.374113	0.044765
57	8	-2.593338	2.718177	4.411763
58	1	-3.199576	2.817227	5.148841
59	1	-3.142671	2.466530	3.631799
60	8	-0.033216	3.290931	1.542943
61	1	-0.463788	3.902007	2.177146
62	1	-0.714929	3.048488	0.887856
63	8	-1.523081	0.118511	3.927212
64	1	-2.179754	0.114862	3.203153
65	1	-1.676279	0.980112	4.346116
66	6	-3.327044	-3.254472	1.134881
67	1	-4.130178	-3.982775	0.970055
68	1	-3.683810	-2.564690	1.900531
69	6	-2.108255	-3.988778	1.679440
70	6	5.167830	-1.280531	0.347683
71	8	6.353811	-1.370234	0.639217
72	7	4.650476	-0.233763	-0.315964
73	6	5.547981	0.766054	-0.861281
74	6	4.798398	1.706151	-1.825366
75	1	4.251483	1.081979	-2.533202
76	1	5.547696	2.267244	-2.383190
77	6	2.643651	2.446514	-0.612763
78	6	3.287627	4.493265	-0.193107
79	1	2.001318	1.578423	-0.628006
80	1	3.253923	5.502957	0.185113
81	1	1.430946	3.745465	0.538641
82	6	3.883087	2.670988	-1.144907
83	7	2.281770	3.618308	-0.009828
84	7	4.275894	3.962176	-0.877519
85	1	6.347406	0.269694	-1.415909
86	6	6.261123	1.586606	0.215679
87	8	7.345091	2.099588	-0.023013
88	7	5.616635	1.731650	1.381245
89	1	6.002318	2.331060	2.089161
90	1	4.693656	1.355058	1.506407
91	6	4.217499	-2.386311	0.741860
92	6	4.757499	-3.654890	0.927774
93	6	2.140212	-3.099301	1.327709
94	6	3.920223	-4.682652	1.308534
95	1	5.813663	-3.812251	0.765737
96	6	2.582532	-4.399924	1.526320
97	1	4.298237	-5.687568	1.438453
98	1	1.894544	-5.179736	1.822247
99	7	2.930709	-2.110563	0.918089
100	6	0.690065	-2.773809	1.540110
101	8	0.055311	-2.086093	0.734488

102	7	0.098269	-3.311948	2.595987
103	1	-2.456241	-4.925124	2.115073
104	1	-1.431986	-4.276422	0.879935
105	6	-1.338406	-3.206028	2.758281
106	1	-1.578514	-3.580386	3.750278
107	1	-1.610816	-2.151726	2.750047
108	1	0.639324	-3.838669	3.259750
109	1	3.740757	-0.351884	-0.764776

[a] E(RwB97XD) = -2887.76007604 Hartree; Zero-point correction = 0.906867; Thermal correction to Energy = 0.965697; Thermal correction to Enthalpy = 0.966641; Thermal correction to Gibbs Free Energy = 0.816783; Sum of electronic and zero-point Energies = -2886.853209; Sum of electronic and thermal Energies = -2886.794379; Sum of electronic and thermal Enthalpies = -2886.793435; Sum of electronic and thermal Free Energies = -2886.943293.

Table S5: Optimized Cartesian coordinates (Å) obtained for the Eu^{III}-DO3A-C3AmpicH system (amide unbound) using DFT calculations.[a]

Center Number	Atomic Number	Coordinates X	Y	Z
1	7	1.018007	2.072277	-0.844049
2	6	2.091020	3.001051	-1.254251
3	6	3.175445	2.382221	-2.108508
4	7	3.964690	1.333319	-1.441544
5	6	4.676942	0.537207	-2.458824
6	6	3.772351	-0.441805	-3.179313
7	7	3.116205	-1.415667	-2.289765
8	6	1.964642	-2.021914	-2.982125
9	6	0.753914	-1.106176	-3.008962
10	7	0.239242	-0.751213	-1.671726
11	6	-0.635553	0.435634	-1.751093
12	6	0.122925	1.734690	-1.967004
13	6	4.918293	1.894336	-0.469926
14	6	4.478380	1.799966	0.985351
15	8	5.337008	1.938204	1.864316
16	8	3.247634	1.572033	1.209930
17	6	4.071227	-2.444191	-1.856564
18	6	4.965555	-1.977604	-0.710405
19	8	6.121205	-2.383103	-0.620121
20	8	4.412729	-1.188918	0.127867
21	6	-0.493052	-1.888705	-1.097662
22	6	0.410965	-2.933882	-0.447502
23	8	0.104096	-4.115350	-0.483191
24	8	1.437175	-2.457698	0.168305
25	1	5.130611	2.948093	-0.680803
26	1	5.867967	1.368123	-0.542038
27	1	4.684692	-2.804086	-2.687359
28	1	3.507780	-3.290322	-1.458647
29	1	-1.131612	-1.517823	-0.292950
30	1	-1.140722	-2.365614	-1.838204
31	1	2.530285	3.407137	-0.344202
32	1	1.678988	3.844353	-1.817772
33	1	3.836552	3.186957	-2.451910

34	1	2.732331	1.953138	-3.004832
35	1	5.142718	1.190685	-3.205746
36	1	5.487630	0.002441	-1.970319
37	1	4.364342	-0.965912	-3.938925
38	1	2.998733	0.101195	-3.717726
39	1	2.223593	-2.282313	-4.014790
40	1	1.718469	-2.956434	-2.482635
41	1	1.001974	-0.188621	-3.536920
42	1	-0.036367	-1.590818	-3.593740
43	1	-1.193596	0.490239	-0.816171
44	1	-1.372171	0.318999	-2.554693
45	1	0.712561	1.677368	-2.879312
46	1	-0.611220	2.529289	-2.136226
47	64	2.264459	-0.239103	0.005064
48	8	3.084180	-1.143279	2.410467
49	8	0.449974	-0.029416	1.700620
50	1	3.871065	-1.550273	2.024317
51	1	3.433793	-0.474447	3.038872
52	1	0.693275	0.617724	2.401189
53	1	0.385666	-0.889459	2.157592
54	8	7.283310	-0.343909	1.184645
55	1	6.616088	0.301452	1.447079
56	1	6.809553	-1.013735	0.665958
57	8	4.192353	0.751343	4.058967
58	1	4.846453	0.434660	4.684620
59	1	4.678027	1.258873	3.371701
60	8	0.751415	-2.644676	2.835893
61	1	1.557683	-2.313653	3.251170
62	1	1.057237	-2.847134	1.931874
63	8	1.584455	1.804861	3.377187
64	1	2.297711	1.883807	2.714694
65	1	2.044137	1.431504	4.136980
66	6	0.241596	2.686115	0.257985
67	1	0.840485	2.627522	1.165170
68	1	-0.641652	2.071907	0.428458
69	6	-0.163922	4.148784	0.049901
70	6	-6.630789	0.024973	-0.883204
71	8	-7.682747	-0.279714	-1.444781
72	7	-5.759738	-0.851553	-0.387814
73	6	-5.884064	-2.291358	-0.511393
74	6	-4.501033	-2.937504	-0.582111
75	1	-4.039949	-2.595831	-1.513330
76	1	-4.625920	-4.015972	-0.665631
77	6	-2.710113	-3.469402	1.195394
78	6	-2.513787	-1.437482	1.987714
79	1	-2.501960	-4.517219	1.073918
80	1	-2.149885	-0.617918	2.585048
81	1	-1.255774	-2.963731	2.678445
82	6	-3.580412	-2.634677	0.558557
83	7	-2.040379	-2.691766	2.101447
84	7	-3.443028	-1.362146	1.065276
85	1	-6.403238	-2.493393	-1.452601
86	6	-6.775981	-2.895116	0.592029
87	8	-6.411473	-3.819126	1.299979
88	7	-7.995227	-2.337294	0.676119
89	1	-8.652553	-2.690993	1.349206
90	1	-8.286291	-1.634509	0.011494
91	6	-6.238532	1.469159	-0.689550

92	6	-7.073324	2.478063	-1.145240
93	6	-4.708884	2.959800	0.113640
94	6	-6.680921	3.789106	-0.943345
95	1	-8.002228	2.227527	-1.636456
96	6	-5.476419	4.039963	-0.307850
97	1	-7.306195	4.608187	-1.272521
98	1	-5.152336	5.055459	-0.124887
99	7	-5.089526	1.703623	-0.068466
100	6	-3.398350	3.149067	0.847063
101	8	-3.110527	2.472224	1.821512
102	7	-2.616274	4.117847	0.341647
103	1	0.674021	4.802934	0.293419
104	1	-0.418785	4.348517	-0.993370
105	6	-1.355520	4.548090	0.913420
106	1	-1.385461	5.632899	1.020887
107	1	-1.279467	4.116656	1.910914
108	1	-2.911336	4.569654	-0.507370
109	1	-4.950770	-0.504770	0.127053

[a] E(RwB97XD) = -2887.75206611 Hartree; Zero-point correction = 0.903666; Thermal correction to Energy = 0.964275; Thermal correction to Enthalpy = 0.965219; Thermal correction to Gibbs Free Energy = 0.809254; Sum of electronic and zero-point Energies = -2886.848400; Sum of electronic and thermal Energies = -2886.787791; Sum of electronic and thermal Enthalpies = -2886.786847; Sum of electronic and thermal Free Energies = - 2886.942812.

Table S6: Optimized Cartesian coordinates (Å) obtained for the CuII-C3AmpicH system (4N) using DFT calculations.[a]

Center Number	Atomic Number	Coordinates X	Y	Z
1	6	-3.815577	3.757254	0.817664
2	1	-3.090869	4.436510	0.360890
3	1	-4.706110	3.751635	0.185011
4	6	-3.241008	2.354993	0.960247
5	6	1.406033	-2.253523	-0.164324
6	8	2.323415	-3.088973	-0.123563
7	7	1.508277	-0.934962	-0.291309
8	29	-0.225450	0.092461	-0.240573
9	6	2.827008	-0.369068	-0.519028
10	6	2.728234	0.899555	-1.366784
11	1	2.276613	0.612423	-2.319820
12	1	3.731228	1.264458	-1.582678
13	6	2.301770	3.314382	-0.590619
14	6	0.264050	3.029715	0.165553
15	1	3.214123	3.835426	-0.817647
16	1	-0.684206	3.250087	0.621912
17	1	1.175137	4.901048	0.264550
18	6	1.943420	2.015271	-0.764401
19	7	1.230102	3.933264	-0.003002
20	7	0.655908	1.856159	-0.291785
21	1	3.421568	-1.092934	-1.089569
22	6	3.621632	-0.139498	0.781216
23	8	4.124508	0.937006	1.066879
24	7	3.743074	-1.230816	1.555131
25	1	4.290009	-1.173755	2.396432

26	1	3.408545	-2.125812	1.221532
27	6	-0.028127	-2.713634	-0.058242
28	6	-0.470290	-4.017225	0.061911
29	6	-2.208707	-1.892637	-0.048088
30	6	-1.842335	-4.233798	0.127299
31	1	0.239178	-4.831022	0.100086
32	6	-2.731560	-3.167533	0.070302
33	1	-2.221122	-5.243120	0.220560
34	1	-3.801215	-3.312723	0.113415
35	7	-0.900870	-1.722613	-0.101504
36	6	-2.986117	-0.597653	-0.146612
37	8	-4.222368	-0.629873	-0.129969
38	7	-2.190445	0.464765	-0.263735
39	1	-2.366451	2.369519	1.618523
40	1	-3.968890	1.695856	1.438242
41	6	-2.849113	1.750155	-0.385816
42	1	-2.177212	2.430722	-0.914713
43	1	-3.748757	1.652471	-1.002057
44	1	-4.096150	4.171442	1.786945

[a] E(UwB97XD) = -2815.5194075 Hartree; Zero-point correction = 0.346556; Thermal correction to Energy = 0.369842; Thermal correction to Enthalpy = 0.370786; Thermal correction to Gibbs Free Energy = 0.293006; Sum of electronic and zero-point Energies = -2815.172851; Sum of electronic and thermal Energies = -2815.149566; Sum of electronic and thermal Enthalpies = -2815.148622; Sum of electronic and thermal Free Energies = -2815.226402.

Table S7: Optimized Cartesian coordinates (Å) obtained for the CuII-C3AmpicH system (3N1O) using DFT calculations.[a]

Center Number	Atomic Number	Coordinates X	Y	Z
1	6	-5.929559	-2.508839	0.338932
2	1	-6.817008	-2.302251	-0.263044
3	1	-5.342690	-3.271016	-0.177964
4	6	-5.110896	-1.245003	0.559635
5	6	1.763633	2.036882	0.451228
6	8	2.700952	2.829961	0.587861
7	7	1.814902	0.707454	0.417075
8	29	0.111714	-0.201948	0.067344
9	6	3.090772	0.039595	0.609696
10	6	2.908113	-1.313208	1.298717
11	1	2.486631	-1.111006	2.286913
12	1	3.887492	-1.762689	1.456393
13	6	2.248682	-3.638540	0.403554
14	6	0.271776	-3.106588	-0.389969
15	1	3.084455	-4.270582	0.643212
16	1	-0.692988	-3.195129	-0.858835
17	1	0.964983	-5.066588	-0.508354
18	6	2.041640	-2.310616	0.602329
19	7	1.124432	-4.115936	-0.220723
20	7	0.794876	-1.998837	0.101258
21	1	3.705980	0.656139	1.273861
22	6	3.875448	-0.072822	-0.711259
23	8	4.192948	-1.144219	-1.203186
24	7	4.193766	1.111416	-1.259012

25	1	4.694175	1.133654	-2.130391
26	1	3.933360	1.973360	-0.800252
27	6	0.354232	2.560237	0.269136
28	6	-0.036735	3.886365	0.280424
29	6	-1.827806	1.849573	-0.139802
30	6	-1.379232	4.170416	0.076013
31	1	0.693689	4.665416	0.442908
32	6	-2.298464	3.148718	-0.140483
33	1	-1.719051	5.196976	0.080412
34	1	-3.339856	3.385058	-0.303672
35	7	-0.542141	1.611802	0.065674
36	6	-2.561695	0.551679	-0.352917
37	8	-1.894507	-0.504277	-0.315378
38	7	-3.856710	0.564754	-0.576710
39	1	-5.703143	-0.501066	1.097548
40	1	-4.236042	-1.466088	1.175136
41	6	-4.644452	-0.647229	-0.762024
42	1	-5.496334	-0.383316	-1.387652
43	1	-4.032299	-1.362837	-1.310203
44	1	-4.343524	1.445321	-0.565715
45	1	-6.259291	-2.926904	1.290147

---

[a] E(UwB97XD) = -2815.9802924 Hartree; Zero-point correction = 0.360035; Thermal correction to Energy = 0.383897; Thermal correction to Enthalpy = 0.384841; Thermal correction to Gibbs Free Energy = 0.304590; Sum of electronic and zero-point Energies = -2815.620257; Sum of electronic and thermal Energies = -2815.596396; Sum of electronic and thermal Enthalpies = -2815.595451; Sum of electronic and thermal Free Energies = -2815.675702.

References:

1 N. Wolf, L. Kersting, C. Herok, C. Mihm and J. Seibel, *J. Org. Chem.*, 2020, **85**, 9751–9760.

2 S. Stoll and A. Schweiger, *J. Magn. Reson.*, 2006, **178**, 42–55.

3 K. Zimmeter, A. Pallier, B. Vileno, M. Sanadar, F. Szeremeta, C. Platas-Iglesias, P. Faller, C. S. Bonnet and A. Sour, *Inorg Chem*, 2024, **63**, 23067–23076.

4 Z. Benkhellat, M. Allali, M. Beley, E. Wenger, M. Bernard, N. Parizel, K. Selmeczi and J. P. Joly, *New J. Chem.*, 2013, **38**, 419–429.

5 J. Peisach and W. E. Blumberg, *Arch Biochem Biophys*, 1974, **165**, 691–708.

6 P. Aisen, A. Leibman and J. Zweier, *J. Biol. Chem.*, 1978, **253**, 1930–1937.

7 Z. Luz and S. Meiboom, *J Chem Phys*, 1964, **40**, 2686–2692.

8 J. H. Freed, *J Chem Phys*, 1978, **68**, 4034–4037.

9 S. H. Koenig, R. D. Brown, M. Spiller, B. Chakrabarti and A. Pande, *Biophys J*, 1992, **61**, 776–785.

10 É. Tóth, O. M. Ni Dhubhghaill, G. Besson, L. Helm and A. E. Merbach, *Magn. Reson. Chem.*, 1999, **37**, 701–708.

11 M. J. ; Frisch, G. W. ; Trucks, H. B. ; Schlegel, Scuseria G. E., Robb M. A.;, J. R. ; Cheeseman, G. ; Scalmani, V. ; Barone, G. A. ; Petersson, H. ; L. X. ; Nakatsuji, M. ; Caricato, A. V. ; Marenich, J. ; Bloino, B. G. ; Janesko, R. ; Gomperts, B. ; Mennucci, H. P. ; Hratchian, J. V. ; Ortiz, A. F. ; Izmaylov, J. L. ; Sonnenberg, D. ; Williams-Young, F. ; Ding, A. ; Petrone, T. ; Henderson, D. ; Ranasinghe, V. G. ; Zakrzewski, J. ; Gao, N. ; Rega, G. ; Zheng, W. ; Liang, M. ; Hada, M. ; Ehara, F. ; Lipparini, F. ; Egidi, J. ; Goings, B. ; Peng, K. ; Toyota, R. ; Fukuda, J. ; Hasegawa, M. ; Ishida, T. ; Nakajima, Y. ; Honda, O. ; Kitao, Nakai H.;, T. ; Vreven, K. ; Throssell, J. A. , Montgomery, J. E. ; Jr.; Peralta, F. ; Ogliaro, M. J. ; Bearpark, J. J. ; Heyd, E. N. ; Brothers, K. N. ; Kudin, V. N. ; Staroverov, T. A. ; Keith, R. ; Kobayashi, J. Normand, R. ; Cammi, J. W. ; Ochterski, R. L. ; Martin, K. ; Morokuma, O. ; Farkas, J. B. ; Foresman, D. J. M. R. L. ; Fox, K. ; Morokuma, O. ; Farkas, J. B. ; Foresman, D. J. Fox, K. ; Raghavachari, A. P. ; B. J. C. ; I. S. S. ; T. J. ; Rendell, M. ; Cossi, J. M. ; Millam, M. ; Klene and C. ; Adamo, *Gaussian16 Revision C.01*.

12 J.-D. Chai and M. Head-Gordon, *Phys. Chem. Chem. Phys.*, 2008, **10**, 6615.

13 F. Weigend and R. Ahlrichs, *Phys. Chem. Chem. Phys.*, 2005, **7**, 3297–3305.

14 M. Dolg, H. Stoll, A. Savin and H. Preuss, *Theor Chim Acta*, 1989, **75**, 173–194.

15 J. Tomasi, B. Mennucci and R. Cammi, *Chem Rev*, 2005, **105**, 2999–3093.

16 M. Regueiro-Figueroa and C. Platas-Iglesias, *J. Phys. Chem. A*, 2015, **119**, 6436–6445.

17 F. Neese, *Wiley Interdiscip. Rev. Comput. Mol. Sci.*, 2012, **2**, 73–78.

18 F. Neese, *Wiley Interdiscip. Rev. Comput. Mol. Sci.*, 2018, **8**, e1327.

19 J. Tao, J. P. Perdew, V. N. Staroverov and G. E. Scuseria, *Phys. Rev. Lett.*, 2003, **91**, 146401.

20 E. Brémond and C. Adamo, *J. Chem. Phys.*, 2011, **135**, 024106.

21 E. Van Lenthe, E. J. Baerends and J. G. Snijders, *J Chem Phys*, 1994, **101**, 9783–9792.

22 E. Van Lenthe, E. J. Baerends and J. G. Snijders, *J Chem Phys*, 1993, **99**, 4597–4610.

23 D. A. Pantazis, X. Y. Chen, C. R. Landis and F. Neese, *J. Chem. Theory Comput.*, 2008, **4**, 908–919.

24 F. Neese, *Journal of Chemical Physics*, 2005, **122**, 34107.

25 G. L. Stoychev, A. A. Auer and F. Neese, *J. Chem. Theory Comput.*, 2017, **13**, 554–562.

26 A. V. Marenich, C. J. Cramer and D. G. Truhlar, *J. Phys. Chem. B*, 2009, **113**, 6378–6396.

27 B. A. Heß, C. M. Marian, U. Wahlgren and O. Gropen, *Chem. Phys. Lett.*, 1996, **251**, 365–371.